Journal of South American Earth Sciences 76 (2017) 25–46

Contents lists available at ScienceDirect

Journal of South American Earth Sciences

journal homepage: www.elsevier.com/locate/jsames

# The role of magma mixing in the evolution of the Early Paleozoic calc-alkaline granitoid suites. Eastern magmatic belt, Puna, NW Argentina

Néstor Suzaño*, Raúl Becchio, Alfonso Sola, Agustín Ortiz, Alexis Nieves, Mirta Quiroga, Gabriela Fuentes

*INENCO-CONICET, Universidad Nacional de Salta, Av. Bolivia 5150, A4400FVY, Salta, Argentina*

ARTICLE INFO

*Article history:*
Received 13 September 2016
Received in revised form
15 February 2017
Accepted 19 February 2017
Available online 22 February 2017

*Keywords:*
Bimodal magmatism
Geochemical modeling
Southern Puna
Active continental margin

ABSTRACT

The outcrops of the Eastern magmatic belt in Puna, NW Argentina, offer an excellent field laboratory to study the interaction processes between magmas of contrasting composition in a plutonic environment. We evaluate the genesis of Cambrian-Ordovician intermediate to acid rocks from the Diablillos Intrusive Complex and the Cerro Bayo area, through detailed geological, petrographic, mineralogical, geochemical, and Nd isotopic analyses in combination with published data. These localities display a great variety of magmatic rocks from diorite/Qz-diorite to two-mica syenogranites with tonalite, granodiorite, monzogranite and Bt-Ttn-leucogranites as mixed products. Major, trace element and whole-rock Nd isotope modeling and petrological data, suggests that magma mixing between hydrous juvenile mantle- and crustal-derived magmas contributed significantly to the geochemical variation of these granites. The estimated proportion of mafic component 0.40–0.67 and 0.14–0.35 in the mixtures may produce the tonalite-granodiorites and monzogranites magmas. The mixing model excludes the predominant influence of fractional crystallization from a mafic magma and local assimilation-fractional-crystallization processes. Isotopic and geochemical comparison between the studied rocks and the magmatic belts in Puna and Tastil batholith suites reveals a marked resemblance. The data suggests that those rocks were probably generated by magma mixing and denotes a regionally and continuous process in a long-lasting (~540-440 Ma) active continental margin. We propose that partial melting of the crust and magma mixing occurred in the lower crust and was possibly triggered by underplated and intraplated hydrous (4.37–5.91 wt% $H_2O$) mafic magmas. The hybrid magmas were emplaced at shallow depth (~8–9 km, 684–727 °C) and occasionally injected either by synplutonic-to late successive pulses of mafic magmas.


## 1. Introduction

Petrologists have invoked a range of processes, including fractional crystallization, assimilation, crustal melting, and magma mixing, to explain the compositional diversity among plutonic rocks of the continental crust. The high-K calc-alkaline granites are often considered as “hybrid” in origin, and involving both mantle and crustal-derived components in their petrogenesis (e.g. Barbarin and Didier, 1992). The interactions between both components either occur at deep crust level related to crustal contamination and/or magma mixing with crustal melts, or by magma mingling and local mixing at the emplacement level. Magma mixing has been mentioned to explain the compositional range of high-K calc-alkaline suites, mainly intermediate to acid composition ($SiO_2$ = 60–75 wt%) that constitute the Western and Eastern magmatic belts in Puna, NW Argentina (e.g. Otamendi et al., 2010). However, this interpretation has been extended from the mixing model of Early Ordovician intermediate to acid plutonism from Valle Fértil-La Huerta (deep-seated crustal section, Otamendi et al., 2009) considering only isotopic and some major elemental composition from Puna magmatic suites. Alternatively, intermediate and acid plutonic rocks from the magmatic belt in Puna, might be the result of crustal recycling processes with minor contribution of juvenile mantle-derived magmas (Becchio et al., 1999; Lucassen et al., 2000; Viramonte et al., 2007) or they could represent fractionated liquids derived from a parental magma of broadly diorite

* Corresponding author. Grupo de investigación de la Unidad de Recursos Geológicos y Geotérmicos vinculado al Instituto en Investigaciones en Energía No Convencional (INENCO), Consejo Nacional de Investigaciones Científicas y Técnicas (CONICET), Salta, Argentina.
*E-mail address:* nestormusic10@gmail.com (N. Suzaño).

http://dx.doi.org/10.1016/j.jsames.2017.02.008
0895-9811/

composition (e.g. Castro et al., 2014; Bellos et al., 2015). In order to account the high $FeO_t$-MgO-$K_2O$, other alternative would the origin by "ferrosilicic magmatism" related to particular petrogenetic models with near-total melting (80–90%) of crustal sources under very high P-T conditions (1000 °C–1200 °C and 1.0–2.0 GPa; Fernández et al., 2008; Castro et al., 2009). Finally, magmatic suite from Puna might results by assimilation of larger amounts of sedimentary, igneous (magmatic enclaves or restite) or local metamorphic country rocks during magma evolution and ascent (e.g. Bahlburg et al., 2016). Thus, considerable uncertainties and controversies remain inconclusive regarding the petrogenesis of the magmatic belts in Puna, particularly on the geochemistry features and volumetrically dominant and spatially extensive intermediate-acid rocks. Coeval mafic and felsic igneous rock associations in the Early Paleozoic Puna magmatic arc and the inference for magma mingling/mixing phenomena is widely reported and documented in the geological literature (e.g. Poma et al., 2004; Coira et al., 2009; Viramonte et al., 2007). However, direct field evidence and detailed study of magma mixing process are scarce (Suzaño et al., 2015). This study addresses on the role of magma mixing process in the origin and evolution of Cambrian-Ordovician intermediate to acid rocks from the Diablillos Intrusive Complex (CID) and the Cerro Bayo area (CBA), southeastern Puna, NW Argentina (Fig. 1). Excellent examples showing the coexistence of magmas of contrasting composition both, in outcrop and mineral scale, give us an opportunity to observe direct evidence for the mixing process. In this paper, we report field, textural, geochemical (elemental and whole-rock isotope Nd), mineral chemistry evidence for magma mixing. For the Nd isotope and mineral chemistry constraints, we focused on Late Cambrian (501 ± 17 Ma, Suzaño et al., 2015) high-K, calc-alkaline suite from the CID. Geochemical (whole-rock major, trace and Sm-Nd data) modeling suggests that mixing is the most likely process explaining the observed compositional variation of the analyzed localities. Also, we applied a mixing test (Fourcade and Allegre, 1981) in order to estimate the proportion of mafic components needed to produce intermediate to acid magmas using a local end-members (hybridized MME and a two-mica syenogranite). The mixing model excludes the predominant influence of fractional crystallization from a mafic magma, as well as local assimilation-fractional-crystallization processes in the genesis of the intermediate-acid magmas. Furthermore, our study, in combination with previously published isotopic compositions and geochemical data reveals marked resemblance between the CID, CBA and those associated with the Eastern magmatic belt in Puna and Tastil batholith (Puna-Eastern Cordillera border, Fig. 1). We interpreted that the mechanisms observed in the CID and CBA related to magma mixing would explain the origin and magmatic evolution of the granites from the Eastern Magmatic belt and Tastil batholith.

## 2. Geological setting

### 2.1. Geological framework and tectonic setting

The pre-Andean basement in the central Andes consists mainly of Proterozoic–Paleozoic metamorphic rocks and associated granites. Tectonomorphic provinces of the central Andean include, from west to east (Fig. 1); (1) the Puna, a relatively high plateau (average elevation ~4 km) region of internal drainage, where Cenozoic sedimentary and volcanic rocks bury Neoproterozoic-Early Paleozoic low to-high metamorphic-igneous basement outcrops. (2) The Eastern Cordillera, a topographically high, externally drained Cenozoic thrust belt with predominantly Lower Paleozoic shelf successions, and Neoproterozoic-Lowermost Cambrian low metamorphic grade basement intruded by Cambrian granites (e.g. Tastil batholith, 540-500 Ma, Hongn et al., 2010 and references therein). Hongn et al. (2010) determined that the called "Tilcarean arc (included of the Cachi-Palermo ranges, Fundiciones, Tipayoc Cañañí intrusives and Tastil batholiths (540-500 Ma, e.g. Hauser et al., 2011)" are considered as Famatinian granites and should not be integrated in the Pampean magmatic arc. (3) Finally, the Pampean Ranges, a topographically high, that extends from NW to central Argentina. The Pampean Ranges consist essentially on Neoproterozoic to Lower Paleozoic medium-high metamorphic rocks, intruded by Cambrian-Ordovician granitic plutons.

The evolution of pre-Andean basement during the Upper Proterozoic and Paleozoic is characterized by convergence along the proto-Pacific margin of Gondwana that generated two main orogenic cycles (Aceñolaza and Toselli, 1981): the Pampean (Upper Precambrian–Lower Cambrian) and Famatinian (Upper Cambrian–Lower Silurian). The Pampean and Famatinian metamorphic and magmatic crystallization ages are regionally and spatially overlapped in the western sections of the orogen (see Lucassen et al., 2011, 2000; Pankhurst et al., 2000; Lucassen and Becchio, 2003). Different authors have proposed diverse models to explain the origin of this basement, and those models involve subduction processes with the formation of magmatic arcs, followed by successive collision of peri-Gondwana or exotic terrenes (e.g. Loewy et al., 2004; Escayola et al., 2011; Hauser et al., 2011). Other authors question these collision models due to the lack of evidence and indicators for this process. Instead, it has been suggested, a geodynamic evolution dominated by intracrustal recycling with minor contributions of juvenile materials (Büttner et al., 2005; Becchio et al., 1999; Bock et al., 2000; Lucassen et al., 2000; among others), or by the intrusion of Early Ordovician mafic magmas at a similar rate to that estimated for present-day magmatic arcs (Otamendi et al., 2010). Lucassen et al. (2000) proposed for the Central Andean basement an evolution in a long-standing high-thermal gradient setting, whereby part of the Pampean and Famatinian cycles are not separate events but one non-differentiable event from 600 to 400 Ma.

At the latitude of the Puna (22°–26°S), the common metamorphic basement (Fig. 1) comprises low-to high-grade rocks with sedimentary protoliths (quartz feldspar-rich greywackes and shales) represented by the Puncoviscana Formation and high-grade metamorphic equivalent (Neoproterozoic to Lowermost Cambrian) and very low-to medium-grade Ordovician pelitic-greywacke units interbedded with felsic and basic volcanic rocks. Radiometric absolute dating of medium-to high-grade metamorphic basement with Sm/Nd and U–Pb metamorphic ages yield 515–500 Ma (Becchio et al., 1999; Lucassen et al., 2000; Lucassen and Becchio, 2003). Abundant Cambro-Ordovician granitic plutons (batholiths) and scarce basic dykes intrude this basement.

### 2.2. Puna magmatic belts

The magmatic belts in Puna (Fig. 1), a thick sequence of dominant acid magmatic rocks (Famatinian Cycle), are represented by two parallel N–S-trending belts; the "Faja Eruptiva de la Puna Occidental" (Palma et al., 1986; referred subsequently as Western belt) and the "Faja Eruptiva de la Puna Oriental" (Méndez, 1972; referred subsequently as Eastern belt). In general, the first one constitutes Ordovician volcanic rocks interbedded with sedimentary sequences and intruded by scarce shallow granites bodies (Pankhurst et al., 1998; Coira et al., 1999; Viramonte et al., 2007). The Western belt represents the northward extension of the Famatinian arc that outcrop along the type localities of the Sistema de Famatina exposed close to the Argentina-Chile-Bolivia borders (e.g. Bahlburg et al., 2016). In the southern most section of the Famatinian arc, deeper levels are exposed with granite–tonalite

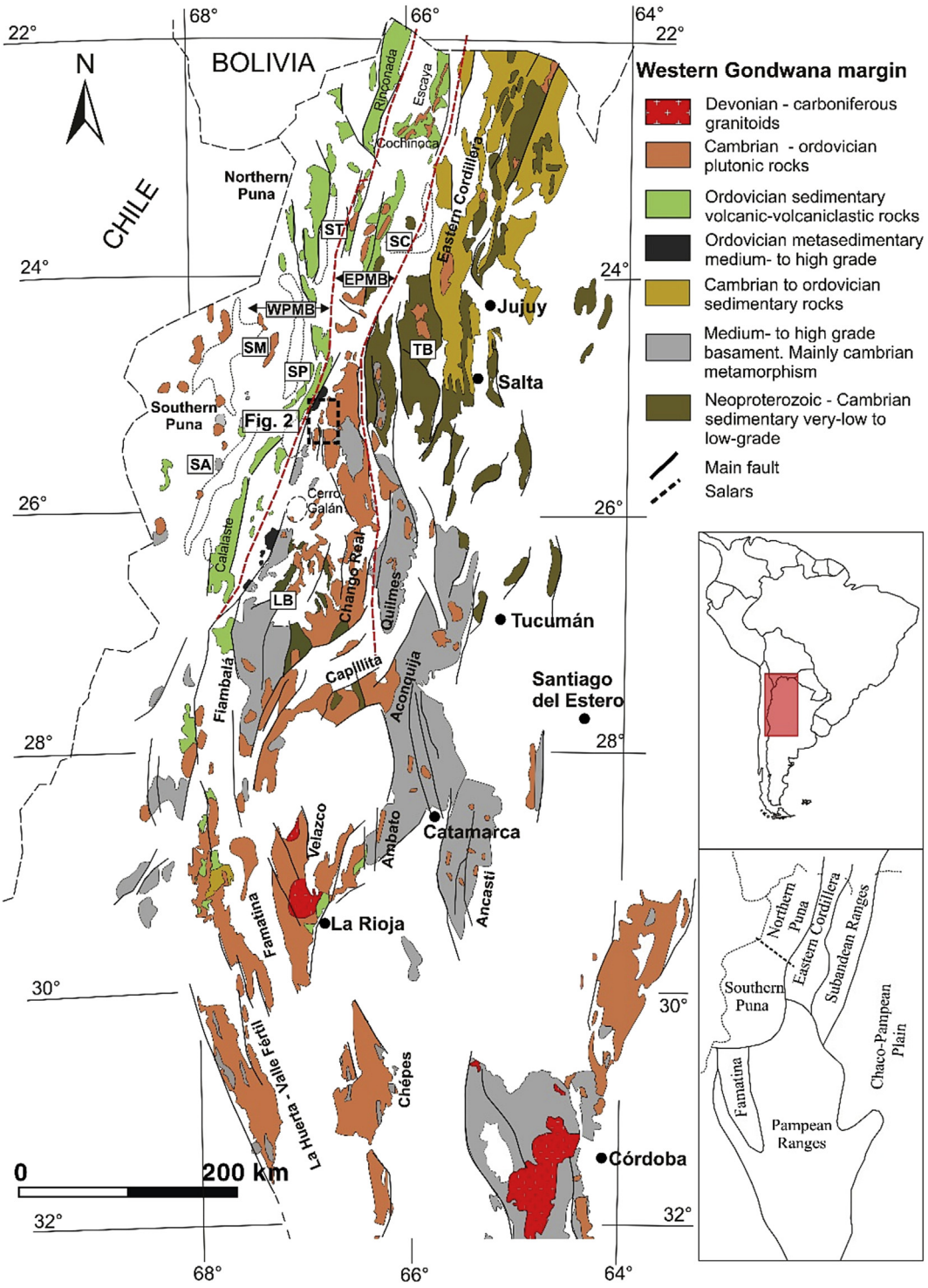


**Fig. 1.** Simplified map of the main outcrops of the Upper Neoproterozoic–Lower Paleozoic basement and magmatic units in central Andes, Argentina. The study area is shown as dashed black lines. Red dashed lines represent generalized boundaries between the Eastern and Western belts. EPMB: Eastern magmatic belt. WPMB: Western magmatic belt. ST: Sierra de Tanque, SC: Sierra de Cobres, TB: Tastil batholith, SM: Sierra de Macón, SP: Salar Pocitos, SA: Salar Antofalla, LB: Laguna Blanca. Modified after Coira et al. (2009), Hongn et al. (2010), Otamendi et al. (2010). (For interpretation of the references to colour in this figure legend, the reader is referred to the web version of this article.)

and associated mafic rocks outcropping (Valle Fértil-La Huerta) as large composite batholiths (Otamendi et al., 2012, 2009; Pankhurst et al., 2000).

The Eastern belt in Puna is considered as part of the Famatinian arc (Famatinian-Puna arc, Loewy et al., 2004; Kleine et al., 2004; Otamendi et al., 2010), in which plutonic, subvolcanic and eruptive facies can be identified. It is a ca. 600 km, N–S trending belt and is divided into two sectors by the Calama–Olacapato–Toro lineament. The northern one (22°–24° S), is characterized by a dominant lavic and subvolcanic bimodal volcanism associated with sedimentary sequences (Coira et al., 2009, 1999; López et al., 2016). Minor bodies of granites (aged from 444 to 480 Ma; Bahlburg et al.,

2016) are also observed in this sector. Some of them contain microgranular mafic enclaves (MME, Didier, 1973) and are intruded by mafic dykes (e.g. The Cobres and Tanque Plutonic Complex; Kirschbaum et al., 2006; Coira et al., 2009). Large volumes of dominant granitic rocks in association with mafic rocks (comprising less than 5 vol%) and volcano-sedimentary sequences characterize the southern sector (24°–27° S) of the Eastern belt. The plutonic rocks are known as "Complejo Eruptivo Oire" ranging in age from Late Cambrian to Late Silurian (500–460 Ma; Viramonte et al., 2007; Insel et al., 2012; among others) with a magmatic peak at ca. 470 Ma. We considered that the studied rocks form part of the Eastern belt (Suzaño et al., 2015).

The granites of the Eastern belt are high-K calc-alkaline and peraluminous associated with mantle-derived mafic rocks (e.g. Viramonte et al., 2007). The bimodal intrusive rocks show negative Nb–Ta, Zr–Hf and Ti anomalies (e.g. Coira et al., 2009; Hauser et al., 2011), which are typical characteristics of subduction-related rocks (e.g. Pearce and Peate, 1995).

## 3. Local geology, field and petrographical characterization

We describe two areas from the Southeastern magmatic belt in order to investigate the intrusive relations between basic and acid magmas. As mentioned above, the localities (Figs. 1 and 2) are (1) Diablillos Intrusive Complex, and (2) Cerro Bayo area. A brief description of the localities and the relevant geological features are given below.

### 3.1. Diablillos Intrusive Complex area (500 Ma). Intrusive units and field relations

The CID constitute the Inca Viejo range located on the eastern edge of the southern Puna, NW Argentina (Fig. 2) and cover an area of ~20 km$^2$. The contacts with the low-to medium metamorphic country rocks are sharp and concordant with N–S striking fabrics. The intermediate to acid granites contain abundant microgranular enclaves (mafic to intermediate in composition) and are intruded by diorite and Qz-diorite stocks and syn-to post-magmatic mafic dikes. Overall, the granites are massive in nature. Locally weak magmatic foliation is evidenced by the preferred orientation of the MME, and synmagmatic pegmatite dykes. Four intrusive units or facies have been distinguished: (1) two-mica syeno- and monzogranite, (2) granodiorite and tonalite, (3) diorite and Qz-diorite, and (4) late mafic dykes. The granodiorite and tonalite rocks represent the dominant unit, comprising the core of the range (Fig. 2). The contact relationships between granites vary from sharp to transitional types. MMEs present in the different units are described separately.

#### 3.1.1. Two-mica syeno- and monzogranite

Granites outcrop in both, the northern and the eastern flank of the Inca Viejo range and consist on dominant monzogranite intruded by scarce syenogranites. Overall, monzogranites consist of gray, porphyritic (up to 2 cm, mainly 1–1.5 cm) with Kfs and Pl phenocrysts immersed in an essentially homogeneous medium-grained Bt-rich matrix (abbreviation minerals after Whitney and Evans, 2010). The mineral assemblage is Kfs (orthoclase and microcline, 13–18%) + Pl (albite–andesine, 24–32%) + Qz (22–37%) + Bt (14–33%) and Ms (<2%). Accessory minerals are Ap, Zrn, Ttn and opaque minerals.

The eastern monzogranite (~0.7 km$^2$) displays transitional contacts with the granodiorite and tonalite units (Fig. 2) and contain abundant enclaves ranging in composition from granodiorite to diorite (MME) and dismembered mafic dykes (Fig. 3a). In thin section, we observe rounded Kfs and Pl phenocrysts with complex internal structures such as a resorption zone (rounded cores) and outer rim (Fig. 4a). The northern monzogranite (~5.7 km$^2$) exhibits scarce enclaves and contains abundant tourmaline miaroles.

The syenogranite comprises less than 5 vol % and intrudes the eastern monzogranite. It is equigranular medium-grained pinkish to white-gray, where the MMEs are absent. The mineralogy consists of Qz (22–37%), microperthitic Kfs (13–18%), Pl (24–32%), Bt and Ms (<5%). Accessory minerals are Ap, Zrn, and Tur. There is no significant microstructural evidence of mineral disequilibrium in the syenogranites. However, the contacts with the monzogranite and mafic rocks are diffuse and occasionally enclose numerous irregular-shapes of MME (up to 2 cm).

#### 3.1.2. Granodiorite and tonalite

These rocks crop out in the core of the Inca Viejo range and cover an area of 11.4 km$^2$. This unit was considered as a hybrid term due to magma mixing between silicic and mafic magmas (Suzaño et al., 2015). Two rocks types are recognized: (1) dark-gray, equigranular fine-to medium-grained tonalities, some places with porphyritic tendency and (2) medium-grained porphyritic granodiorite. Both types show abundant MME, dismembered mafic dykes and rare tonalitic-granodioritic enclaves and abundant content of Bt (often constitute clots).

Tonalities are dark gray colored in hand specimens. The mineral assemblage is Pl (33–42%) + Qz (22–32%) + Bt (26–36%) ± Kfs (up to 4%) and Amp + Ap ± Ep and opaque minerals as accessory. Equigranular tonalite is constituted by a fine-grained groundmass of small typically unzoned laths of Pl, Bt, Ap, Amp and interstitial Qz (Fig. 3b). Porphyritic tonalite shows Pl phenocryst with a wide range of textures such as complex zoning with rounded cores and Bt-mantled. Ap is a ubiquitous accessory mineral and occurs as acicular crystals in the rock matrix (Fig. 4b). Scarce fine-grained Amp crystals show subhedral-anhedral shape.

Porphyritic granodiorites show ovoidal white Kfs, Pl, and blue Qz phenocrysts (up to 1.5 cm). The main minerals are Qz (22–34%), Pl (albite–andesine; 21–42%), Kfs (orthoclase and microcline, 4–14%), Bt (26–34% and exceptionally 41%) ± muscovite. Minor/accessory phases are Ttn, Ep, Ap, Zrn and opaque oxides. Some microcline phenocryst develops a thin rim of Pl (rapakivi mantling texture). Pl phenocryst forms both individual grain and glomerocrysts. Pl varies in size from 2 to 4 mm and exhibits zoned and Bt-mantled structures.

#### 3.1.3. Mafic igneous rocks, enclaves and field relations with the host granites

Mafic rocks outcrops cover an area of ~0.3 km$^2$ and vary from diorite to Qz-diorite. They are widely distributed in the CID as intrusive bodies (stocks), isolated enclaves (MME), dismembered bodies (Fig. 3a) and late mafic dykes. These rocks are dark gray-to dark green and vary from equigranular fine grained to porphyritic, although, locally it can be observed slightly porphyritic ones. All examined samples contain Pl (36–52%), Amp (45–52%), Bt (up to 15%) with scarce Qz (2–8%) and rare Kfs xenocryst. Accessory or minor minerals include Ap, Zr, Ttn and Ep and opaque minerals.

Dismembered bodies intrude into the monzogranite, granodiorite and tonalite and show ellipsoidal–spheroidal to tabular shapes with up to 5 m in thick/diameter. In general, the contacts with the host granites are sharp. In addition, it is observed compositionally zoned bodies typically mantled by a dark, 2-cm thick, fine-grained Bt-rich rinds along mafic intrusions and enclaves. Besides, some dismembered bodies contain xenocrysts (blue Qz ocelli and Pl; Fig. 4c) and acid micro-enclaves (Hibbard, 1995). The set of NE–SW striking late mafic dykes cut both the monzogranite and the medium metamorphic grade country-rocks at

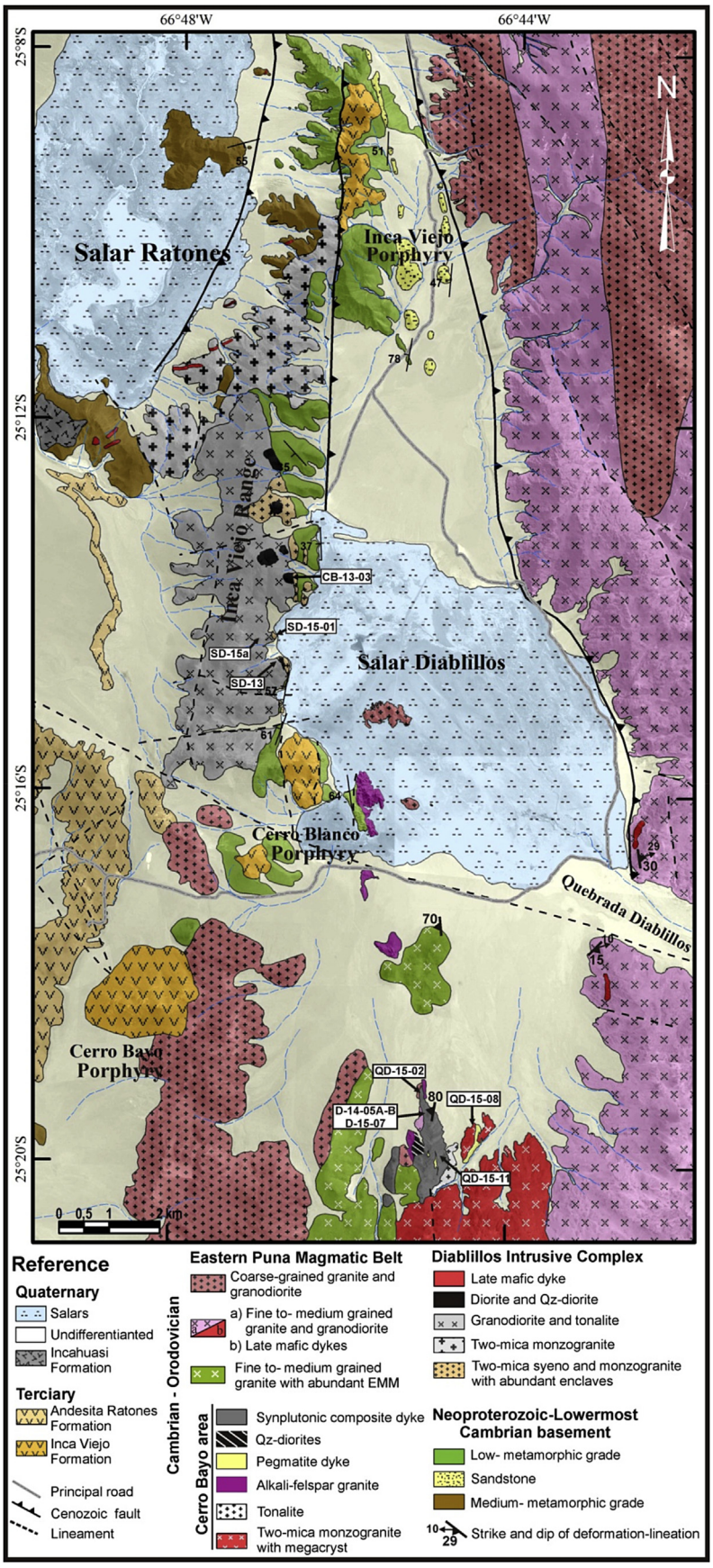


**Fig. 2.** Geological map of the Salar Diablillos zone in the western sector of the Eastern belt and location of the new analyzed samples (modified from Suzaño et al., 2015). See text for details.

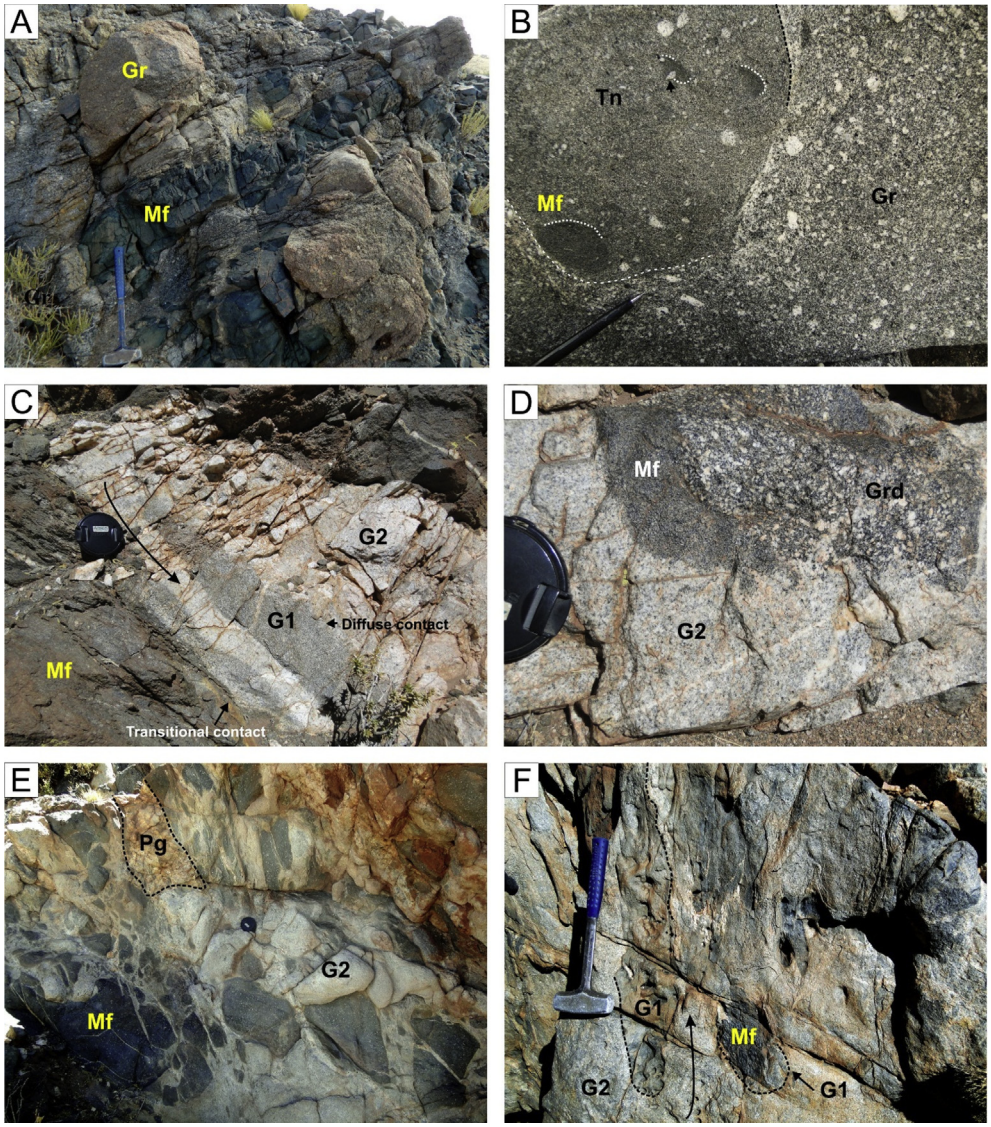


**Fig. 3.** It shows the field relations of the intermediate to acid granitoids from the studied localities and associated mafic rocks. (A) Partially dismembered synplutonic mafic dyke (Mf) and (B) rounded tonalitic (Tn) multi-component magmatic enclave (tonalite + MME) hosted in granodiorite (Grd) from CID. (C) Cerro Bayo composite dyke: Mafic rocks intruded by two-mica syenogranite dykes generating granites with variable composition (monzogranites G1 and syenogranite G2). (D) multi-component magmatic enclave (granodiorite + MME) partially digested by the syenogranite (G2). (E) MME swarm related to two-mica syenogranite (G2) and late pegmatite (Pg) intrusions into mafic dyke and (F) intrusive syenogranite (G2) into the synplutonic dykes generating two distinct compositional enclaves (G1 and Mf).

the eastern flank of Inca Viejo range (Fig. 2). The dykes contain Pl phenocrysts (zoned and sieve type) surrounded by a fine-grained matrix composed of Pl, Amp, with scarce Bt and Qz.

Mafic (MME) to intermediate enclaves show a random distribution within the CID and are especially abundant along the eastern flank of Inca Viejo range (Fig. 2). The MME are gray to dark green, equigranular to porphyritic and show typical igneous textures. They have various shapes, including rounded, ellipsoidal, discoidal, elongated and can reach up to 2 m in diameter. The contacts with its host granites are dominantly sharp yet transitional and diffuse contacts are occasionally found. Additionally, isolated feldspar and Qz phenocrysts are observed either as xenocryst into the MME, or cutting the contact between MME and the host granite. Those xenocrysts have the same features that the phenocrysts commonly found dispersed in the granitic host (e.g. ocellar blue Qz and rounded feldspar). Overall, enclaves consist in a fine-grained groundmass constituted by Amp, elongate laths of Pl, Bt, and small amounts of Qz, Ttn, Zrn, Ilm, Ep, and Ap. In porphyritic samples, Pl phenocrysts show complex oscillatory zoning with repeated resorption surfaces. Also present, are small amounts of poikilitic Pl with hornblende inclusion and large glomerocrysts. Poikilitic and zoned Pl grains are abundant along the contact between the MME and the host granites. Ttn is ubiquitous and tends to form relatively fine anhedral crystals.

Compositionally zoned (double enclave) and multi-component enclaves are also present (Fig. 3b). The first one has a dark, xenocryst-poor center, surrounded by lighter “hybrid” zones relatively rich in Kfs and Qz xenocrysts. The cores of these enclaves may represent retained blobs of the probably non-hybrid mafic magma (e.g. Barbarin and Didier, 1992), whereas the outer zones resulted from the mixing of varied proportions of acid and mafic magmas. The multi-component enclaves are scarce and consist in dispersed xenocryst-free MME enclosed in an intermediate composition matrix, which contains xenocrystic feldspars similar to phenocrysts in the medium-grained host granite (Fig. 3b).

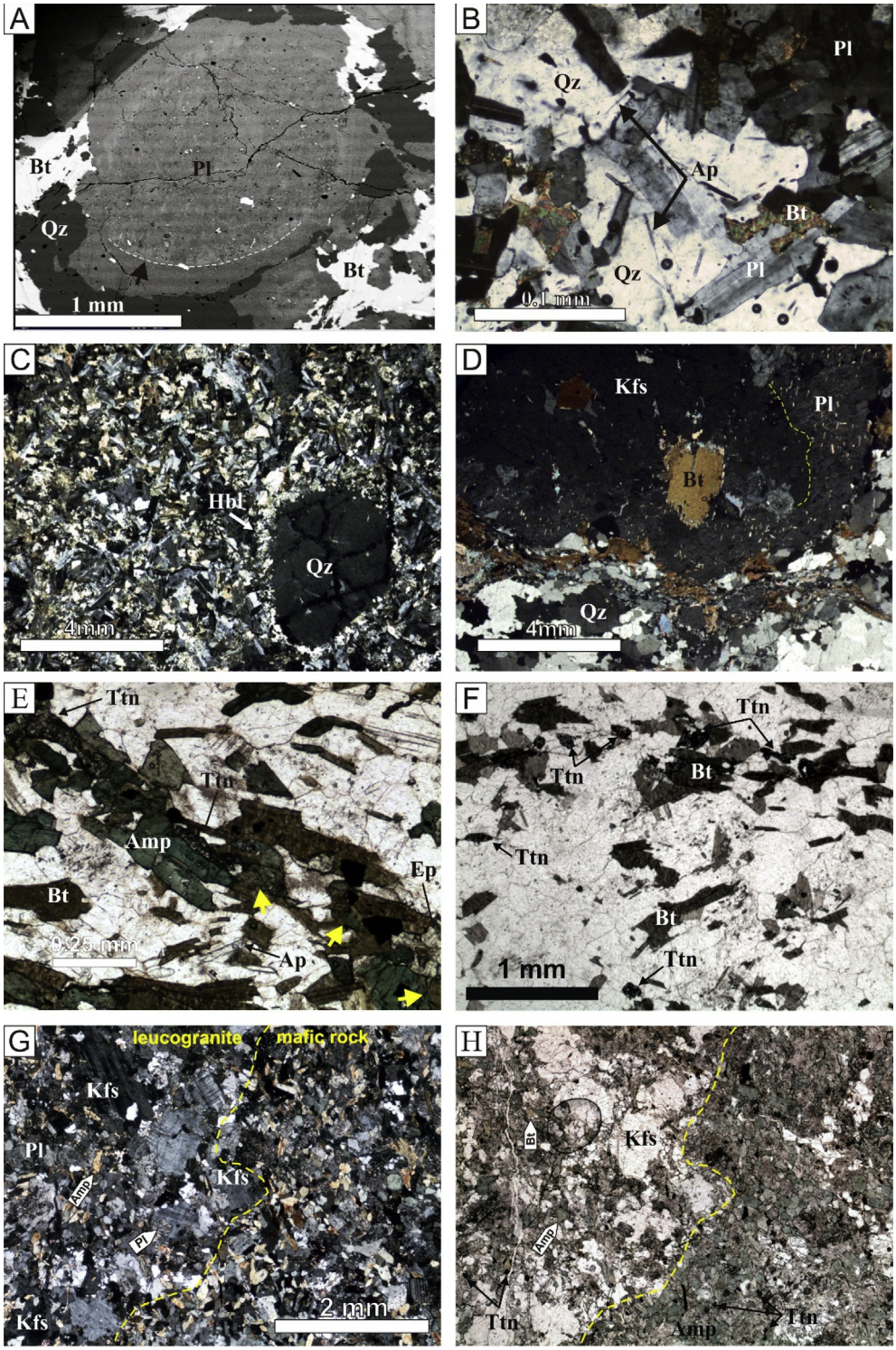


**Fig. 4.** Photomicrographs showing the textures of the representative samples. (A) A BSE image of a Pl grain from the granodiorite sample SD-18-07 (CID) exhibiting a core–mantle–rim structure. Note the resorbed core surrounded by a rim of more Ab-rich composition. (B) Fine-grained equigranular tonalite (CID) with lath-shape Pl and acicular Ap. (C) Fine-grained MME with a dominance of Amp, Pl, and scarce Qz. Note the quartz grain with reacted rim (quartz ocelli). (D) Two-mica monzogranite (QD-15-08) with Kfs megacryst surrounded by Pl (rapakivi texture). (E) Amp-Bt Qz-diorite (QD-15-02) showing the conversion of Amp to Bt texture. (F) Bt-Ttn monzogranite from CBA. Note the anhedral Ttn associated with Bt and individual grain. (G) and (H) Transitional contact of two-mica syenogranite-mafic rock in the synplutonic composite dyke. Note the Amp and Ttn xenocryst in leucogranite coming from a mafic rock and conversion of Amp to Bt texture. B, C, D and G images were taken in cross-polarized light.

### 3.2. Cerro Bayo area (CBA)

It is located in the SW of the Inca Viejo range (Fig. 2), western sector of the southern segment of the Eastern belt. The CBA is constituted by an elongate synplutonic composite dyke body enclosed within granites (alkali-feldspar and megacrystic monzogranite), granodiorites and tonalities assigned to the Eastern belt (Hongn and Seggiaro, 2001).

Alkali-feldspar granite crops out along the western side of the area and it is in transitional contact with small bodies of granodiorite. The granite is pinkish-gray, equigranular medium-grained and constituted by Qz + Pl + Kfs + Bt + Ms. The accessory minerals consist on Zr, Ap, Ep and opaque minerals. Two-mica monzogranite is a distinctive porphyritic granite intruded by pegmatites dykes and crop out in the eastern sector of the area (Fig. 2). It is gray in color and encloses scarce rounded dark-gray microgranular enclaves and k-feldspar megacrysts up to 7 cm in size. These are included in a coarse-grained groundmass constituted by kfs + Pl + Qz + Bt + Ms and accessory Zrn, Ap and opaque minerals. In some case, the Kfs megacrysts develop a thin outer rim composed by Pl (rapakivi texture, Fig. 4d), which is common in magma mixing environment (Hibbard, 1995). The granodiorite is dark-gray and contains abundant dark-gray MME with ellipsoidal shapes, sizing from 4 to 30 cm and irregular to diffuse contacts with the host rock. Granodiorite shows porphyritic texture and consists mainly on Pl phenocryst included in a fine-grained groundmass composed by Pl, Bt, Qz and Kfs as well as accessory minerals such as Ap, Zrn, and opaque minerals.

The tonalite is medium-gray, equigranular fine-grained and crop out in the eastern sector of the area (Fig. 2). It is composed by Pl + Bt + Qz + Kfs + Ap + Zrn + opaque minerals and contains abundant metasedimentary xenoliths and igneous dark-gray microgranular enclaves (2–20 cm in diameter). Scarce schlieren composed mostly by Bt can be observed. The MMEs ranging in shape from spheroidal to ellipsoidal–ovoidal, and they have few centimeters in diameter (up to 30 cm). The contacts between the enclaves and the host rocks are mainly sharp-rounded and irregular or diffuse.

### 3.2.1. Synplutonic composite dyke

This unit crop out in the central and northern sector of CBA (Fig. 2) and cover an area of 0.8 km × 2.0 km. Synplutonic composite dyke body is characterized by exhibiting an excellent example of mafic-acid rocks association (where both melts occupy the same conduit). It included Qz-diorite (Bt-Qz-diorite and Amp-Qz-diorite) and a wide range of leucogranites (syeno to monzogranite) with abundant MME and acid enclave inclusions (Fig. 3c–f). All these magmatic units have transitional contacts with one another.

In the northern sector of CBA crop out dark-gray, equigranular fine-grained Bt-Qz-diorite (Fig. 3c). The mineral association is Amp + Bt + Pl + Qz + Ttn + Ep + Aln + Ap + Zrn and opaque minerals. Qz-diorite is characterized by its abundant Bt content (Table 1) and exhibits conversion of Amp to Bt texture (Fig. 4e). Commonly, Bt rimming Amp crystals with diffuse contact type (Fig. 4e). This texture is characteristic of magma mixing process (Hibbard, 1995), although it is very common in a fractionating magmatic system. Ttn is abundant and occurs as anhedral-subhedral grain associated with Bt and Amp. Tabular bodies of leucogranites (two-mica syenogranite) up to 5 m in size intrude the Bt-Qz-diorite (Fig. 3c). Leucogranites are white to grayish, medium-grained, with partially digested mafic, granodioritic enclaves and fewer common multi-component enclave (MME-granodiorite, e.g. Collins et al., 2000) (Fig. 3d). The contact between the leucogranite and the Qz-diorite varies from sharp to transitional. In the latter one, the leucogranite shows local mixing with the host generating a thin MME-rich zone.

Fig. 3e y f illustrates the relations between various lithological components from the central sector of the body. Successive acid dykes cut the previous mafic dykes and generate variable leucogranites types (G2 = Bt-Ttn syenogranite and G1 = Bt-Ttn monzogranite). The Bt-Ttn syenogranite (G2 in Fig. 3c–f) frequently occurs either homogeneous tabular bodies or dismembered mafic magmas (MME swarm, Fig. 3e) and Bt-Ttn-monzogranite (G1, Fig. 3f). Overall, leucogranites are white to dark-gray, equigranular fine to medium-grained. Similar mineral association (Qz + perthitic Kfs + Pl + Bt + Ttn + Zrn + Ep + Aln + Ap and opaque oxides) constitutes the leucogranites (G1 and G2), but a progressive variation in the modal proportion especially in the biotite-muscovite-titanite association can be observed (Table 1). It is noted that the Ms is present only some leucogranites (D-14-5A and QD-15-04 samples, Table 1) and disappears in the others ones (QD-15-11 and QD-15-11B samples, Table 1) together with the increasement of Bt and Ttn contents. Abundant fine-grained anhedral Ttn (Fig. 4f–h), rare zoned Pl phenocryst and anhedral Amp particularly along felsic-mafic rock contacts (Fig. 4g–h), are a salient feature of leucogranitic rocks. Micro-phenocrysts of Pl vary from subhedral to anhedral, and the same grains show rounded core-rim structures. Fine-grained prismatic Ep and Aln surrounded by a mantle of Ep are common.

The Am-Qz-diorite occurs both as a homogeneous dyke and as MME included in leucogranites (Fig. 3e). In general, they vary from porphyric to equigranular fine-grained and the contacts with the host are sharp to transitional. In some places, homogeneous Am-Qz-diorite shows irregular leucogranitic intrusions up to 1 m in thickness. Other homogeneous dykes contain spectacular pipes of acid (7 × 15 cm in diameter) rock. MME are subrounded to elongate, flame-shape in some places, and frequently aligned parallel to flow-zones with meter scale within the leucogranitic dyke (Fig. 3e–f). The enclave-host rock contacts vary from sharp/irregular to diffuse over a distance of a few centimeters. Rounded MME are mostly 10–30 cm in diameter (Fig. 3f) but range from a few millimeters to 1.0 m in size.

## 4. Results

### 4.1. Mineral chemistry. Diablillos Intrusive Complex

We emphasize in the plagioclase phenocrysts disequilibrium textures (e.g. zoning or resorption surface, Fig. 5a–d) because it can

**Table 1**
Modal composition of CBA units. *Selected samples for whole-rock major and trace elements geochemistry.

| Sample | Rock type | Qz | Kfs | Pl | Ms | Bt | Amp | Ttn | Opq | Ep | Ap | Tur |
|---|---|---|---|---|---|---|---|---|---|---|---|---|
| QD-15-08* | Two-mica monzogranite with megacrysts | 36 | 12 | 23 | 2 | 24 | | | <0.5 | | 1.0 | <0.4 |
| QD-15-01 | Alkali-feldspar granite | 31 | 60 | 5 | 2 | 1 | | | | <1.0 | <0.1 | <0.5 |
| D-14-5A* | Two-mica syenogranite | 40 | 45 | 14 | 1.7 | 1.3 | | | <0.3 | <0.4 | <0.3 | |
| QD-15-04 | Two-mica syenogranite | 38 | 45 | 7 | 5 | 9.8 | | <1.0 | <1.0 | 2.1 | <0.4 | |
| QD-15-11* | Bt-Ttn syenogranite | 42 | 23 | 11 | | 16 | | 4.3 | 1.1 | 2.0 | 1.0 | |
| QD-15-11B | Bt-Ttn monzogranite | 37 | 18 | 19 | | 20 | | 2.5 | 1.0 | 1.2 | 1.0 | |
| QD-15-02* | Bt-Qz-diorite | 11 | | 46 | | 14 | 19.5 | 5.5 | 1.8 | 1.3 | 1.1 | |
| D-14-07 | Amp-Qz-diorite | 9 | | 36 | | | 46 | 4.7 | 1.5 | 1.0 | 0.8 | |
| D-14-5B* | Amp-Qz-diorite | 6 | | 28 | | | 55 | 8.0 | 1.5 | 0.5 | 1.1 | |
| D-14-06 | Amp-Qz-diorite | 7 | | 28 | | | 58 | 5.0 | 1.1 | 1.4 | 1.0 | |

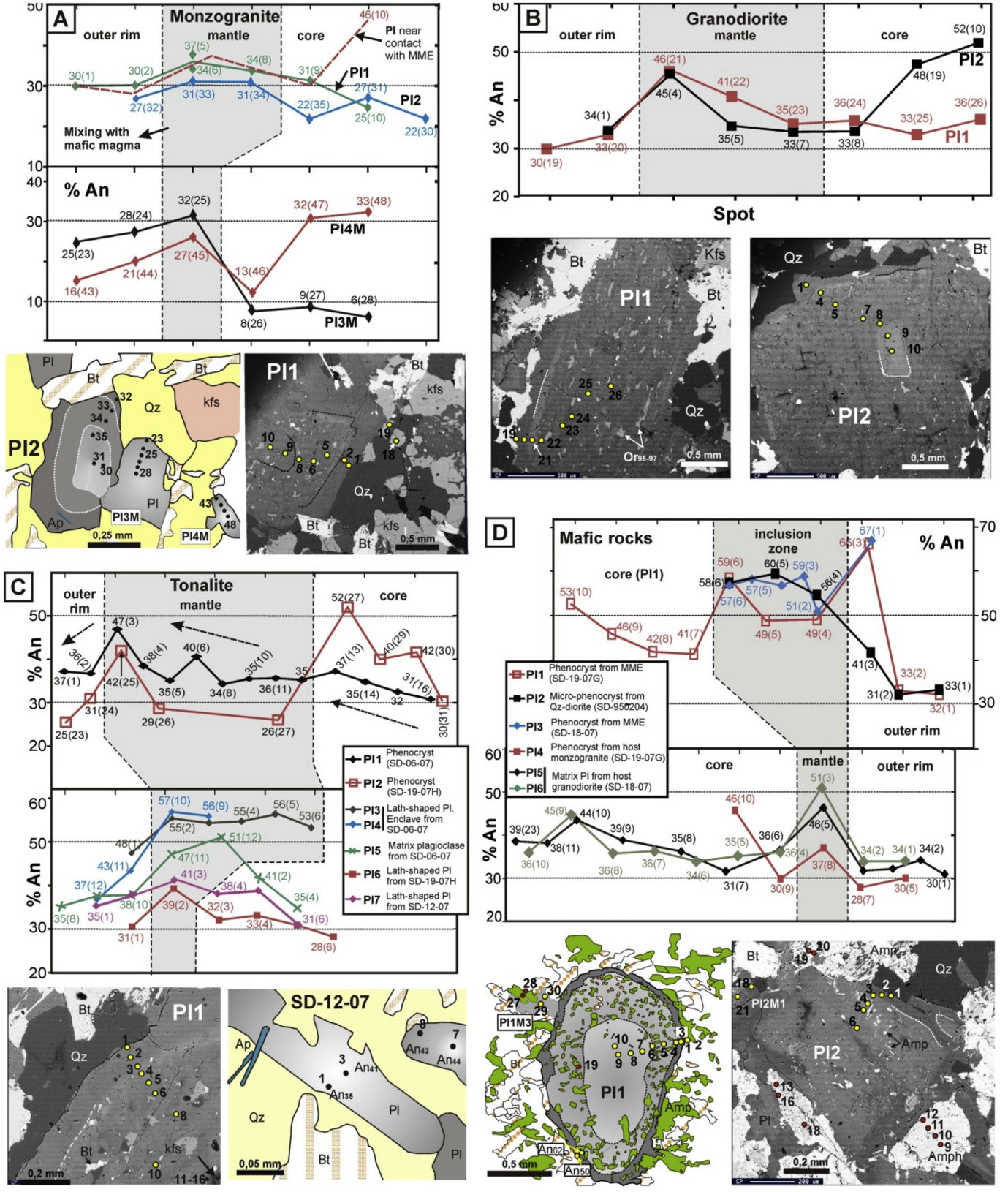


**Fig. 5.** Schemes and backscattered electron (BSE) images and corresponding traverses section for An of representative Pl from the enclaves, mafic intrusive body and host intermediate to acid granitoids. Numbered dots show the locations of microprobe analyses. (A) Pl phenocryst and matrix from host monzogranite sample SD-19-07B, exhibiting a core–mantle–rim structure because of variation in calcium contents. Note the variable An content of Pl from the monzogranite matrix. (B) Pl phenocrysts from granodiorite sample SD-19-07E comprising a core, An-rich mantle and rim. Pl2 shows calcic core and a wide patchy mantle. (C) Pl phenocryst and smaller lath-shape Pl of the matrix from tonalities bodies (SD-12-07 y SD-19-07H) and enclaves (SD-06-07). Note the abrupt decrease of calcium value from the core to the mantle in the Pl phenocryst and from mantle to the rim in lath-shape Pl. (D) Pl phenocrysts from MME (SD-19-07G and SD-18-07), mafic intrusive body (D-950204) and host intermediate to acid granitoids. Note that most Pl exhibits a core–mantle–rim structure and featured a An-rich mantle and calcium-poor rim (contamination with evolved magmas). An-rich mantle of Pl from the host granitoids point to mafic melt injection process.

shed light on the extent of open-system processes such as magma mixing (e.g. Pietranik and Koepke, 2014).

#### 4.1.1. Plagioclase zoning and composition

Based on observations of twelve samples, most of the Pl phenocrysts show three zones (core–mantle–rim structures): rounded-shape core, an An-rich mantle and an outer rim in contact with the mineral matrix. Optical zoning is not obvious for all Pl grains.

*4.1.1.1. Monzogranite.* Pl phenocrysts (up to 5.0 mm, SD-19-07B) mostly show slightly reverse compositional zoning from the core to mantle (Fig. 5a) followed by An-poor outer rim. Some cases, cores show resorption surface. In addition, it can be observed normal and reverse zoning in smaller Pl (0.3 mm) and Kfs ($Or_{94-95}$) from the matrix. In general, the Pl matrix (Pl3M and Pl4M, Fig. 5a) may include similar zones to those found in the Pl phenocryst (core, An-rich mantle and rim). Most Pl cores (Pl1, Pl2, Pl4M) ranging in values from $An_{22}$ to $An_{33}$ (Table A1) and one Pl grain from the matrix (Pl3M) has a notably lower An content ($An_6$ to $An_8$, albite). Furthermore, near the contact between the MME and the host monzogranite, Pl phenocryst exhibits a core with a An value ($An_{46}$) compatible with the core of Pl phenocryst of the MME (SD-19-07G, Fig. 5d). A normally zoned outer rim surrounding the An-rich mantle shows lower calcium values and decreases from $An_{30}$ to $An_{16}$ (Oligoclase).

*4.1.1.2. Granodiorite.* Pl phenocrysts (SD-19-07E, Fig. 5b) show compositional zoning in core–mantle–rim (Pl1 and Pl2) structures. Pl1 and Pl2 cores show normal zoning, but dissimilar An content varying from $An_{36}$ to $An_{33}$ and $An_{52}$ to $An_{33}$ respectively. The Pl1 and Pl2 show a An-rich mantle with reverse zoning increasing from $An_{33}$ to $An_{46}$. Then, the outer rim decreases in calcium value in both Pl ($An_{30-34}$, Fig. 5b). Smaller analyzed Pl grains from the matrix (Pl3, Table A1) do not exhibit compositional zoning, and their An content ($An_{32-33}$) is similar to those Pl phenocrysts in the outer rim.

*4.1.1.3. Tonalite.* Three samples from the contact between the mafic tonalitic enclave (SD-06-07) and the main body (SD-12-07 y SD-19-07H) were analyzed (Table A1). Most Pl from the matrix has lath-shape and exhibit core–rim structures. Pl phenocrysts show complex zoning in core–mantle–rim structures, where individual rims exhibit a reverse pattern (Fig. 5c). The Pl1 phenocryst (SD-06-07) shows rounded core with low calcium values varying from $An_{30}$ to $An_{37}$, although it can be observed a notable increase in Pl2 $An_{30}$ to $An_{57}$ (SD-19-07H). Mantles show a reverse pattern from $An_{35}$ to $An_{47}$ and $An_{26}$ to $An_{36}$ values in Pl1 and Pl2 respectively. A normally zoned rim that surrounds the mantle decreases from $An_{47}$ to $An_{25}$.

Lath-shaped Pl from both equigranular tonalite (SD-12-07) and matrix of porphyritic ones (SD-06-07 and SD-19-07H) are optically homogeneous. However, they may include either core-mantle-rim (Pl5 and Pl6 = enclave and Pl7 = matrix from the host) or mantle-rim (Pl4 and Pl5) zoning pattern. Thus, Pl5, Pl6 and Pl7 (SD-19-07H, Fig. 5c) have a reverse calcium-poor core ($An_{28}$ to $An_{41}$) and a high An zone ($An_{39}$ to $An_{51}$) surrounded by a normally zoned rim ($An_{31}$ to $An_{38}$). Matrix Pl rims show very similar An contents to the Pl phenocryst rims (Pl2-Pl6 and Pl1-Pl5 phenocryst-matrix plagioclase couple). Plagioclases from the mafic tonalitic enclave (Pl3 and Pl4) exhibit a high An mantle ($An_{53}$ to $An_{57}$) surrounded by a calcium-poor normally zoned rim ($An_{48}$ to $An_{37}$).

*4.1.1.4. Mafic rocks and host granites.* Three samples from the EMM-host rocks contact (SD-19-07G and SD-18-07) and an intrusive body (D-950204) were analyzed (Table A1). Most Pl phenocrysts show complex zoning in core–rim structures (except Pl1 showing core–mantle–rim structures). It is also observed, rounded and irregularly shaped cores containing highly variable An ($An_{41}$ to $An_{60}$). Pl1 shows core ($An_{53}$ to $An_{41}$), mantle ($An_{56}$ to $An_{49}$) with Amp inclusion and outer rim ($An_{66}$ to $An_{33}$) structure. Individual rims exhibit normal zoning pattern, but the general trend always decreasing in An content from core to rim. Cores from Pl2 (D-950204) and Pl3 (MME from SD-18-07) shows similar behavior with $An_{51}$ to $An_{60}$ values. However, the outer rim from Pl3 shows an abrupt increase in An ($An_{67}$), whereas Pl2 exhibits a normal pattern (Fig. 5d). On the other hand, the lower An content of the outermost rim Pl1 (MME) and Pl2 (mafic body, $An_{31}$ to $An_{33}$) are consistent with anorthite content from monzogranite and granodiorite (Fig. 5a–b). Pl of the matrix of intrusive body sample (D-950204, PlM1) exhibits very similar zoning patterns that the phenocryst grain (Pl2): cores enriched in An ($An_{58}$) surrounded by a calcium-poor rim ($An_{33-34}$). The plagioclases in the matrix of the MME (SD-19-07G) exhibit normal and slight reverse zoning pattern (PlM1 and PlM2 respectively, Table A1). Most of the matrix Pl and phenocrysts of the host granites exhibit core-An-rich mantle–rim structures. Pl matrix of (Pl5 and Pl6) the host granodiorite (SD-18-07) shows a rounded shape (resorption surface) core with wavy-patchily zoning pattern ($An_{31}$ to $An_{45}$) followed by An-rich mantle ($An_{46}$ to $An_{51}$). The rim composition varies from $An_{30}$ to $An_{34}$, similar to the outer rim of Pl phenocryst from the granodiorite (Fig. 5b). Pl phenocryst of the host monzogranite (SD-19-07G, Fig. 4a, d) shows normal-wavy zoning. The core has high An ($An_{46-30}$) and is consistent with the An values observed in Pl phenocryst of hosted MME. Mantle shows a peak of An ($An_{37}$) and decreases in the rim from $An_{30}$ to $An_{28}$.

#### 4.1.2. Amphibole

Representative microprobe Amp analyses from MME (SD-19-07G) and intrusive body (SD-950402) are given in supplementary Table A1. All Amp grains analyzed show compositional variation between core and rim, including those occurring as inclusion in plagioclase (Pl1, Fig. 5c). They belong to the calcic amphibole group with CaB = 1.78–2.00 pfu., (Ca + Na)B = 1.86–2.00 pfu. NaB <0.5 pfu, and can be further classified as MHb according to Leake et al. (1997) classification scheme (Fig. A1a). However, Amp grains show a slight tendency toward the actinolite member and one amphibole rim from SD-950402 plotted in the field of tschermakitic members. Overall, Amps from the intrusive body show higher Ti ($TiO_2$ = 0.20–1.4 wt%) than MME ($TiO_2$ = 0.12–0.82 wt%). Cores and adjacent zones show a progressive Mg enrichment (slight negative slope in Mg/(Mg + Fe) vs. $TiO_2$, Fig. A1b) and decrease abruptly towards crystal edges. In contrast, rims of the amphibole inclusion in plagioclase phenocryst (Pl1, Fig. 5d) and one grain from the matrix are Mg-rich than that in core.

#### 4.1.3. Biotite

Bt is the common Fe–Mg mineral in every facies that makes up the CID, and 55 spot analyses from MME-rich samples and Qz-diorite (Fig. A1c-f) are given in Appendix Table A1. All Bt grains yield the typical composition of metaluminous calc-alkaline granites (Fig. A1c-d; Abdel-Rahman, 1994). Nevertheless, Bt from more evolved terms plots in or close to the peraluminous field (e.g. typically Bt of migmatites, Sola, 2012). In terms of Fe/Mg + Fe ($X_{Fe}$) and Ti, Bt of the MME-monzogranite host (SD-19-07b), Qz-diorite (D-950204) and tonalities (SD-19-07h and SD-12-07) are characterized by low $X_{Fe}$ (0.34–0.51) and Ti (0.16–0.21 pfu) compositions. On the other hand, Bt from the monzogranite (SD-12-18), granodiorite and tonalitic enclave-host (SD-06-07) show higher $X_{Fe}$ (0.54–0.61) and lower Ti (0.22–0.23 pfu) compositions. In addition, all Bt grains show positive arrange in $X_{Fe}$ vs. Ti pfu (Fig. A1e) where those from the tonalite-granodiorites plot in the middle area

between diorite and monzogranite ones. However, most Bt from mafic tonalitic enclave and host plot close to the monzogranite domain (Fig. A1e), although, they show lower $K_2O$ (8.9–9.7 wt%) content than Bt from monzogranite (11.2–11.6 wt%). The MgO and $FeO_t$ negative correlation (Fig. A1f) suggests that Mg↔Fe substitution prevailed during Bt evolution. Thereby, monzogranite Bt close to the contact with MME shows higher content of $X_{Fe}$ (0.49–0.53), Fig. A1f) than those in free-MME monzogranites ($X_{Fe}$ = 0.55–0.58).

### 4.2. Whole-rock geochemistry

Whole rock geochemical data including major and trace elements on ten representative samples from two localities (five from CID and five from CBA) are given in Table A2 and their locations are given in the map of Fig. 2. In addition, previously published data from the CID are plotted in Figs. 6–11 diagrams for comparison.

#### 4.2.1. Whole-rock major- and trace-elements compositions

According to Frost and Frost's (2008) classification scheme, the CID and CBA rocks are magnesian-type (Fig. 6a) and it extends close to the ferroan-type in granites. Rocks show calc-alkalic and alkali-calcic affinities (Fig. 6a–b), typical feature of subduction-related rocks (Fig. 6c). Intermediate to acid rocks yield $SiO_2$ and $Na_2O + K_2O$ contents of 59.7–76.4 wt% and 4.8–8.9 wt% respectively. These values are very close to the Eastern belt ($Na_2O + K_2O$ = 4.6–9.5 wt%), Tastil batholith ($Na_2O + K_2O$ = 6.5–8.6 wt%) and anatectic granites ($Na_2O + K_2O$ = 4.5–8.9 wt%). On the other hand, intermediate to acid rocks of the CID and CBA show higher $Na_2O + K_2O$ content than typical Cordilleran-type batholiths from Sierra Nevada ($Na_2O + K_2O$ = 4.9–7.6 wt%). In addition, intermediate to acid rocks from the Eastern belt and the Tastil batholith show relative enrichment in $K_2O$ and minor $Na_2O$ content than typical calc-alkaline values of the Sierra Nevada batholith. These geochemical

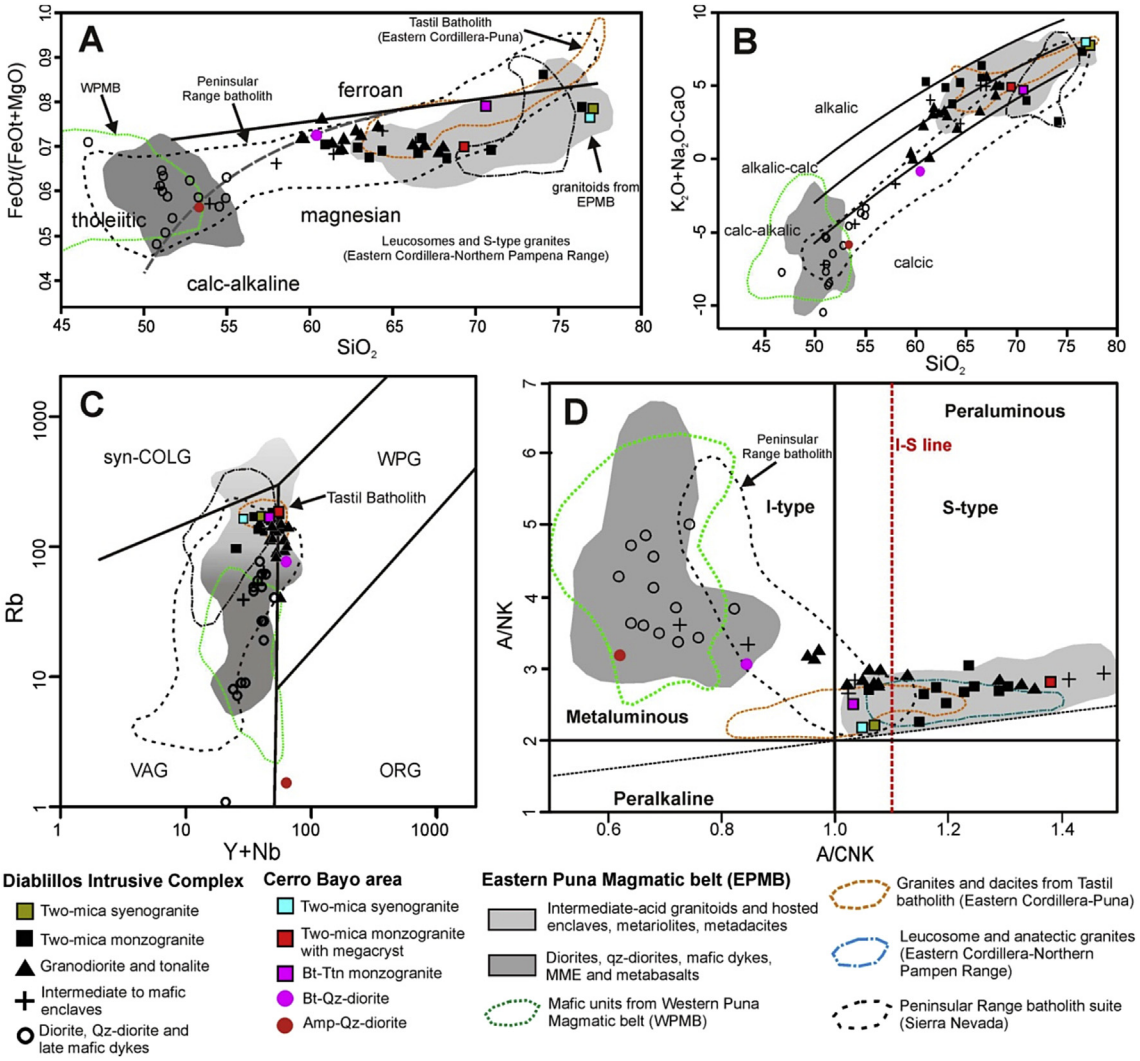


**Fig. 6.** Representative diagrams illustrating the geochemical characteristics of studied localities. (A) Plots of Fe-number ($FeO_t/(FeO_t + MgO)$) vs. $SiO_2$ diagrams are after (Frost and Frost, 2008). (B) $Na_2O + K_2O$–CaO vs. $SiO_2$ after Frost and Frost (2008). (C) Rb–Y + Nb diagram after Pearce et al. (1984), VAG: volcanic-arc granites, syn-COLG: syn-collisional granites. WPG: within plate granites, ORG: ocean-ridge granites, (D) A/CNK vs. A/NK diagram. The I–S line is after Chappell and White (2001). CID published geochemical data after Suzaño et al. (2015); Becchio et al. (1999); Damm et al. (1994, 1990) and Lucassen et al. (2001). Eastern Puna magmatic belt after Damm et al. (1994); Coira et al. (1999, 2009); Becchio et al. (1999); Kirschbaum et al. (2006); Viramonte et al. (2007); Bahlburg (1990); Hauser et al. (2011); Damm et al. (1990. 1994); Lucassen et al. (2001) and López et al. (2016). Data of mafic units from Western Puna magmatic belt after Kleine et al. (2004) and Zimmermann et al. (2014). Data from Tastil batholith (Eastern Cordillera-Puna border) after Hauser et al. (2011) and Damm et al. (1990, 1994). Data for the leucosome and anatectic granites from Eastern Cordillera and Northern Pampean ranges after Sola et al. (2013) and Lucassen et al. (2001). Data for the Peninsular Range batholith in North America are from Lee et al. (2007).

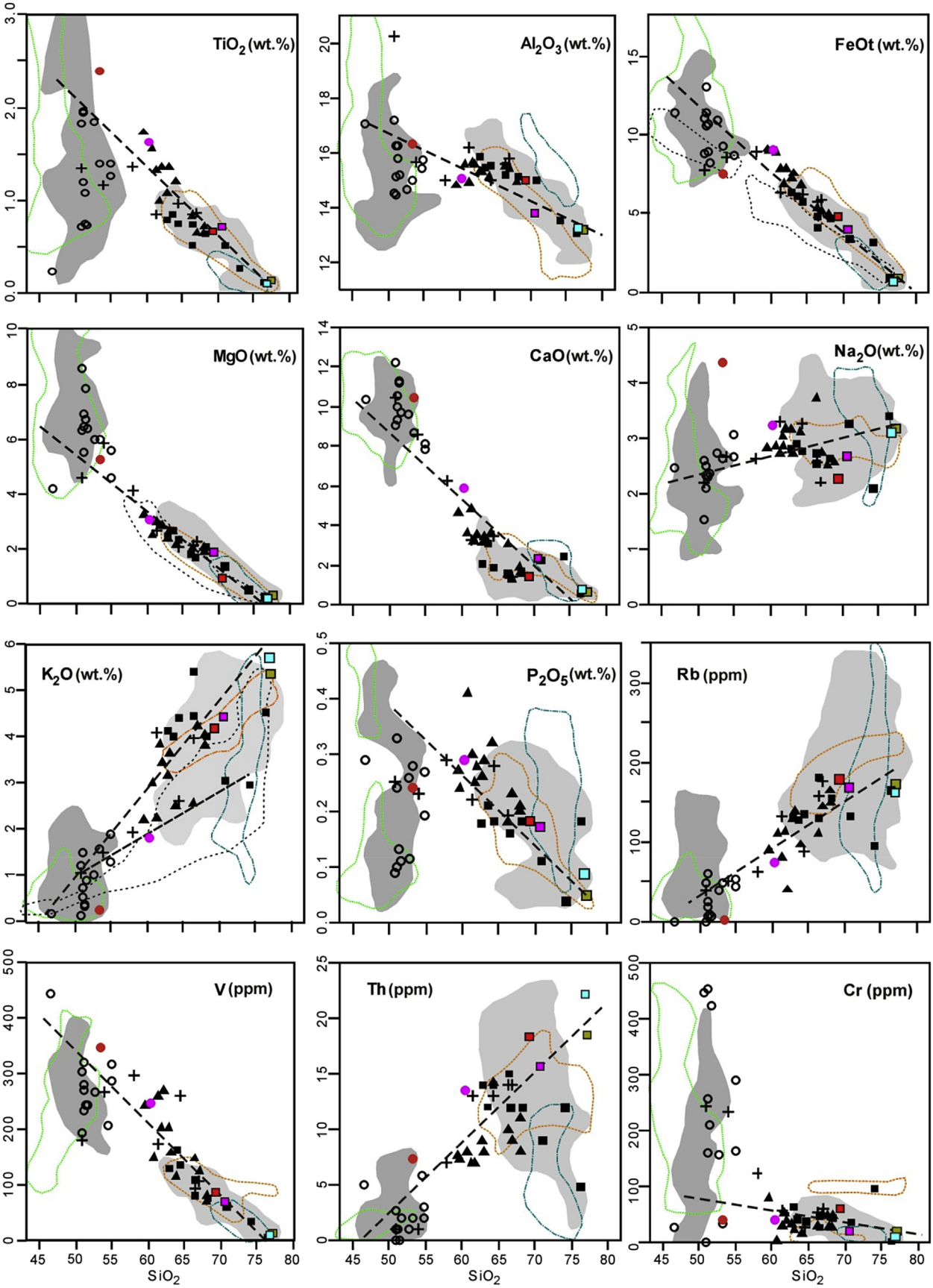


**Fig. 7.** Major and trace elements binary diagrams showing the compositional variation of the mafic rocks, intermediate-acid granitoids and their hosted enclaves from CID and CBA. Compositional field plotted includes the Eastern belt, mafic plutonic units from the Western belt and the Tastil Batholith from Puna-Easter Cordillera border and crustal-derived granites from Easter Cordillera-Northern Pampean ranges. In $FeO_t$, MgO and $K_2O$, the compositional field of typical Cordilleran batholiths from the Sierra Nevada are plotted. Symbols and data are the same as in Fig. 6.

features remain along the Famatinian-Puna paleo-arc and were highlighted by previous researchers (e.g. Ducea et al., 2015; Suzaño et al., 2015).

Most mafic rocks from studied localities included those from the Puna magmatic belts show calcic to calc-alkalic and tholeiitic-magnesian geochemical affinities (Fig. 6a and b). In terms of alumina saturation index (A/CNK; Fig. 6c), intermediate to acid rocks from CID and CBA varies from strongly peraluminous to weakly metaluminous. Most of these rocks plot between the I–S line and A/CNK = 0.93. The Eastern belt, Tastil batholith and anatectic granites show similar distribution patterns, but the Tastil batholith is extended up to A/CNK = 0.8.

*4.2.1.1. Diablillos Intrusive Complex.* The CID suit and its enclaves show a large range of $SiO_2$ content (Table A2). Mafic rocks and MME (Fig. 7) show moderate to high $FeO_t$ MgO and CaO contents, low $K_2O$ and a wide range of $Al_2O_3$, $TiO_2$, $P_2O_5$ and $Na_2O$ for a narrow range of $SiO_2$ (46.6–54.9 wt%). These features are consistent with the distribution pattern observed in mafic rocks from the Western and Eastern belts (Fig. 7). In addition, the CID mafic rocks display flat to slight negative rare earth element (REE, (La/Sm)N = 0.98–2.23, N denoting chondrite-normalized values, Table A2) patterns in the chondrite normalized diagrams. They show enrichment of light rare earth elements (LREEs, (La/Yb)N = 1.02–3.63), nearly flatten heavy rare earth elements (HREEs. (Gd/Yb)N = 1.02–1.47) and moderate negative Eu anomalies (Eu/Eu* = 0.80–0.96) (Fig. 8a). In the primitive mantle normalized trace-element diagram, the CID mafic rocks show enrichment in LILE, slight Pb as well as depletion in Nb, P and Ti (Fig. 8b).

Granodiorites and tonalities (included enclaves) plot in a middle position between mafic rocks and more evolved samples (syeno-to monzogranite) according to the variation diagrams (Fig. 7). They yield higher MgO, $FeO_t$ and more scattered $K_2O$ in intermediate-acid granitoids values compared to the Sierra Nevada batholiths (Fig. 7). This is a distinctive feature of the Puna and Tastil batholith magmatism. Granodiorites and tonalities show parallel chondrite normalized RRE patterns and moderate enrichment of LREEs ((La/Yb)N = 4.01–6.46). In addition, they display moderate negative Eu anomalies (Eu/Eu* = 0.55–0.76) (Fig. 8a; Table A2). In the spider diagram (Fig. 8b) granodiorites and tonalities exhibit enrichment in LILE together with depletion in Nb and Ti.

Two-mica syeno-monzogranite samples have intermediate to high contents of $SiO_2$, $Na_2O$, MgO, $FeO_t$, $Al_2O_3$ and a large range of $K_2O$, Rb, Th and Ba contents (Fig. 7). Furthermore, they show low CaO, $TiO_2$, $P_2O_5$, Cr and V contents. The $K_2O$ abundance of granites is clear higher than the Sierra Nevada batholiths (Fig. 7) and its large range distribution is consistent with the observed in natural (e.g. Sola et al., 2013) and experimental anatectic melts (Patiño Douce and Harris, 1998; at 0.6–0.8 GPa). In chondrite-normalized REE plots, the granites exhibit relatively high concentration of LREEs ((La/Sm)N = 2.88–3.32) and low values of HREEs (Gd/Yb)N = 1.01–2.03) resulting in weakly steep patterns ((La/Yb)N = 3.77–9.73) (Fig. 8a). Granites yield moderate negative Eu anomalies (Eu/Eu* = 0.50–0.64). In the primitive mantle normalized trace elements diagram (Fig. 8b); the rocks have obvious LILE (Cs, Rb, Ba) enrichment relative to HFSE coupled with Nb depletion and marked negative Sr, Ti and P anomalies.

*4.2.1.2. Cerro Bayo area.* The mafic sample (Amp-Qz-diorite, D-15-05B) shows low contents of $SiO_2$, $K_2O$, Th, Cr and moderate to high $Na_2O$, MgO, $TiO_2$, $FeO_t$, $Al_2O_3$, Sr and V (Table A2). The Bt-Qz-diorite (QD-15-02) sample yields lower $Al_2O_3$, $TiO_2$, CaO, MgO, Sr and more $K_2O$, $FeO_t$, Rb, Ba than mafic samples. It shows compositional equivalence with the typical tonalite from CID (Fig. 7).

Bt-Ttn leucogranite (QD-15-11) is featured by strong enrichment in $FeO_t$ (3.98 wt%), $P_2O_5$, $TiO_2$, $Al_2O_3$, CaO, moderate MgO (0.94 wt%), V and lower $K_2O$ (4.43 wt%), $Na_2O$ and Th values than uncontaminated Two-mica syenogranite (Fig. 7, Table A2). These values are consistent mainly with the Pl (some as phenocryst), Bt, Ttn, Ep and Ap modal mineralogy enrichment (Table 1). Two-mica syenogranite (D-14-5A) exhibits typical crustal-derived acid magma composition. In the variation diagrams, it plots very close or into the crustal-derived melt field (Fig. 7). However, two-mica syenogranite shows lower $Al_2O_3$ and higher Th than those anatectic melt. Megacrystic monzogranite (QD-15-08) show similar geochemical behavior to Bt-Ttn monzogranite (from intrusion interior composite dyke) in the most geochemical variation schemes (Figs. 6–8). In addition, these rocks coupled with hybrid Bt-Qz-diorite, plot in an intermediate position between mafic–two-mica syenogranite (linear trend) in the variation diagrams (Fig. 7).

Chondrite-normalized patterns for the megacrystic granite, two-mica syenogranite and Bt-Ttn monzogranite (Table A2; Fig. 8c) exhibit parallel distribution. Moderate enrichment of LREEs ((La/Sm)N = 3.36–4.88), near-flat HREEs ((Gd/Yb)N = 0.94–1.32) and medium negative Eu anomalies (Eu/Eu* = 0.36–0.54) are observed. Two-mica syenogranite yields lower total REEs and pronounced Eu anomalies (Eu/Eu* = 0.36) than Bt-Ttn monzogranite. The Bt–Qz–diorite and Amp–Qz–diorite samples display similar high total REE (ΣREEs = 140–187 ppm) and sub-parallel REE patterns. No prominent Eu anomalies (Eu/Eu* = 0.69–0.77), moderate enrichment of LREEs ((La/Sm)N = 2.08–2.63) and near-flat HREEs ((Gd/Yb)N = 1.01–1.06) are observed. All rock types have negative Nb, P and Ti anomalies and enrichment in Ba, Rb, Th and K (Fig. 8d).

*4.2.2. Whole-rock major- and trace-elements variation*

Major oxide contents are plotted on the Harker variation diagrams (Fig. 7) to investigate their bulk-chemical evolution and its geochemical affinities with the Eastern belt and the Tastil batholith. Collectively, all samples from CID and CBA have pronounced-linear trends (Table 2) of decreasing $FeO_t$, CaO, and MgO, V, near-lineal $TiO_2$, Sr and near-lineal increasing $K_2O$, Rb, Ba with increasing silica content (Fig. 8, Table 2). However, the $P_2O_5$, $Al_2O_3$, and $Na_2O$, Cr values exhibit greater scattering (mainly in mafic members) and less correlation with $SiO_2$. Similar bulk-chemical evolution is noted for the Eastern belt suit and the Tastil batholiths (Fig. 7). Bt-Qz-diorite, tonalities, granodiorites and most monzogranites overlap within the $SiO_2$ range of 59–69 wt%, always plotting in the middle between the two-mica syenogranite and mafic rocks.

Decreasing $TiO_2$, $FeO_t$, CaO, MgO and increasing $K_2O$ with increasing $SiO_2$ may partially be related to Bt, Amp and Pl fractionation during differentiation of parental hydrous mafic magmas. However, modal content and concentration of these elements in granites (e.g. high $FeO_t$, MgO, $K_2O$ or high modal Bt (up to 30%) cannot be explained in terms of the simple closed-system fractional crystallization. In addition, the less contaminated mafic magmas in the Puna magmatic belts coupled with Valle Fértil-La Huerta suit have very low $K_2O$ contents (0.2–1.0 wt%; Otamendi et al., 2010; Ducea et al., 2015; Suzaño et al., 2015) and the covariation between $K_2O$ and $SiO_2$ is hard to explain by closed-system fractional crystallization. Scattered distribution of $K_2O$ in evolved granites is similar to those related to crustal-derived acid magma compositions. Crust-derived melt can undergo fractional crystallization or variable degrees of melt–residuum separation process (Sola et al., 2013) resulting in compositional variations.

CID and CBA rocks show progressive enrichments of Ba, Rb (Fig. 8) and decrement of Zr, Y, Cr and Ni (not shown) with increasing $SiO_2$ content. On the other hand, the mafic members show a high scattering for these elements. Negative correlation between Y and $SiO_2$ observed for the mafic samples (Fig. 7) may be due to the early crystallization of Ca-rich accessory phases such as

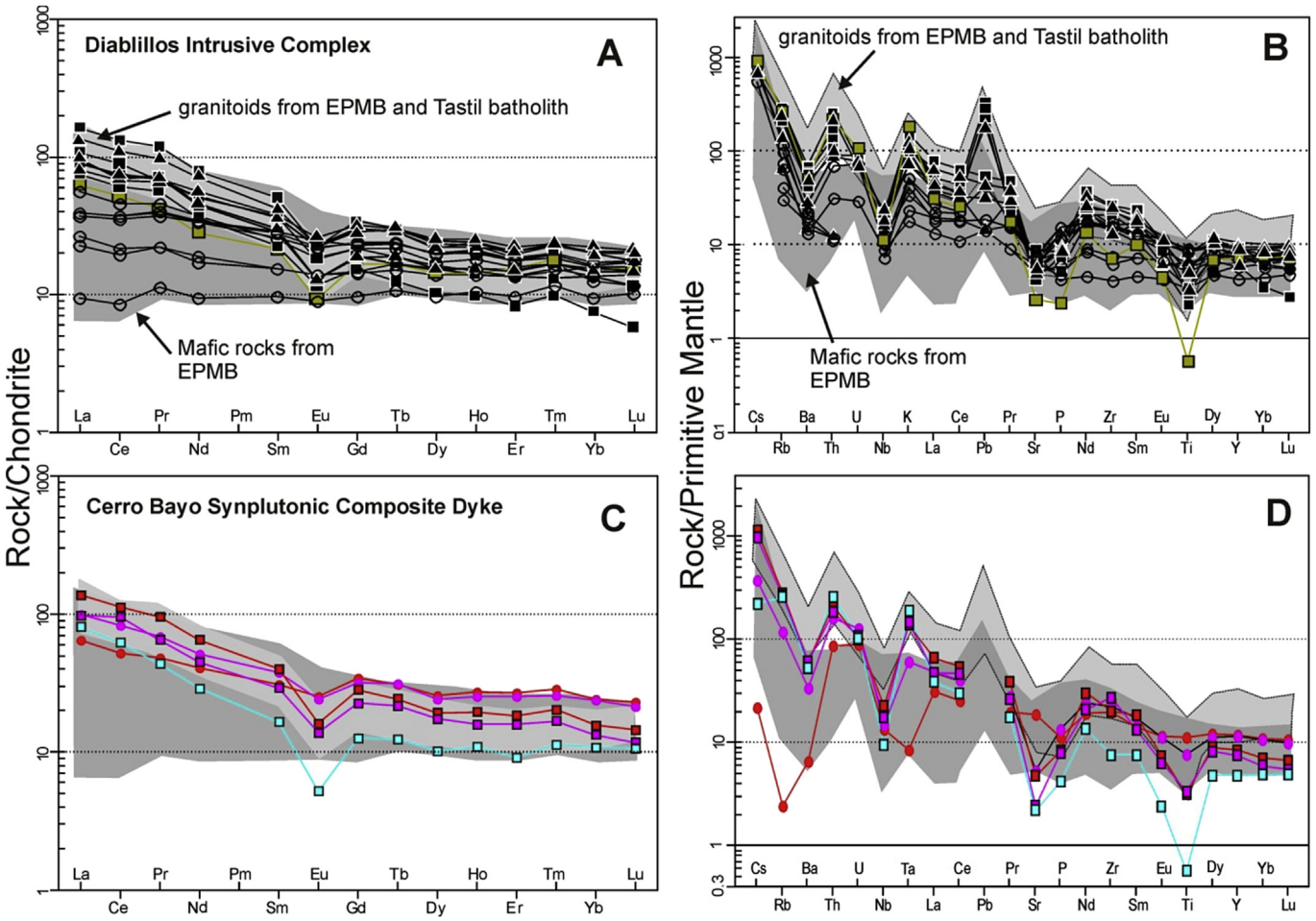


**Fig. 8.** Chondrite-normalized REE patterns (Nakamura, 1974) and primitive mantle-normalized spider diagrams (Sun and McDonough, 1989) of the intermediate to acid and mafic rocks from the (A) y (B) Diablillos intrusive complex, (C) and (D) Cerro Bayo synplutonic composite dyke. Symbols and data are the same as in Fig. 6.

apatite and sphene, which agrees with the observed depletion in $P_2O_5$ with increasing $SiO_2$. However, the same mafic samples are rich in Y (D-14-05B), which agrees with the modal sphene content (Table 1).

### 4.3. Whole-rock isotopic compositions and variations

Five representative samples from CID (including one dioritic intrusive body, two MME, one tonalitic enclave and one granodiorite), and its country rocks were selected for Nd isotopic analysis (Table A3 and Fig. 9). The data (recalculated at 500 Ma) are described together with previous data from the CID (Damm et al., 1994; Becchio et al., 1999) and compared with others magmatic rocks from the Eastern and Western belts, the Tastil Batholith and fertile metamorphic basement from Eastern Puna and Eastern Cordillera (Fig. 9).

CID granites yield εNdt values from −4.7 to −7.5 and two-stage Nd model ages (TDM) of 1.5–1.8 Ma (Fig. 9). Dioritic intrusive bodies and MMEs yield a wider range of εNd values. The diorite yields εNd value of +1.7 and TDM value of 1.040 Ma. MMEs show strongly negative εNd values from −4.3 to −7.4 and largely overlapping with those of the granites hosts. Probably it is related to partial or completes isotopic equilibration of MME with their host; such has been claimed in many studies (e.g. Elburg, 1996). However, enclaves and host preserve distinctive whole-rock chemical signatures. Granodiorite and tonalite isotopic compositions show homogeneous values from −2.4 to −3.9 and TDM values of 1.363–1.456 Ma. Overall, granites display the lowest Nd isotopic composition and plot within the field of the Eastern belt and the Tastil batholith granites and extend towards the field of western Puna-Eastern Cordillera metamorphic basement (Fig. 9). The dioritic intrusive body from the CID is consistent with the mafic isotopic composition of the Western and Eastern belts. On the other hand, Nd composition and model ages of intermediate and acid rocks exhibit average values suggesting the mass contribution of two contrasting sources. This feature is known as a mixed-age (DePaolo, 1981) where the model ages of tonalities and granodiorites from CID may result from mixing mafic and acid rocks (Fig. 9).

## 5. Discussion

In this study, we systematically analyzed two groups of bimodal igneous rocks from the Diablillos Intrusive Complex and Cerro Bayo area. Each group is represented by intermediate-acid magmatic rocks, which either carry enclaves (intermediate to mafic) or are intruded by sin-to post-mafic dykes. Their field relationships suggest generalized input of mafic magma into the acid magma chamber with variable degrees of magma mixing and mingling. Diverse contact types (sharp to transitional), morphology and geometry of mafic dykes suggest intrusion of mafic dykes into felsic magmatic chambers with variable stages of crystallization (Barbarin, 2005). Similar typical bimodal magmatism with magma

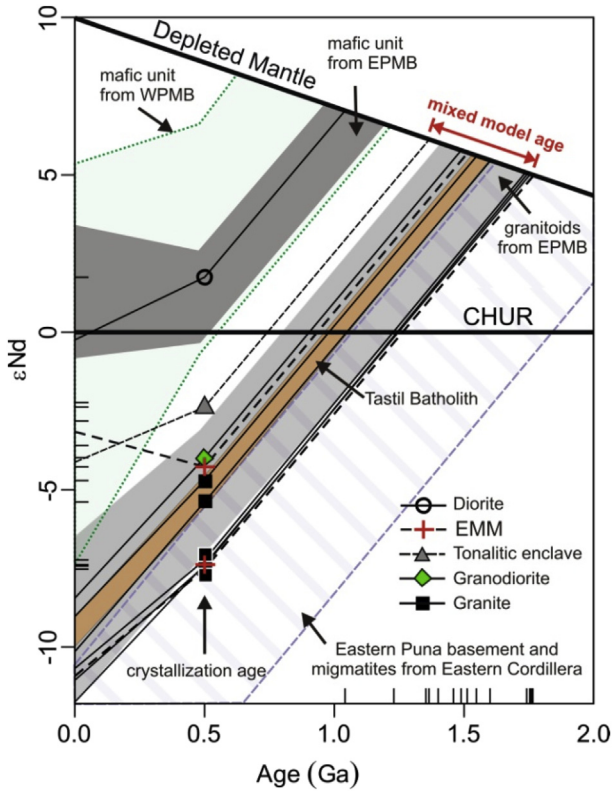


**Fig. 9.** Plots of $\varepsilon_{Nd}$(500 Ma) versus Sm–Nd model ages (Ga) for the granitoids and their hosted enclaves from the CID. Sm–Nd model ages compared to depleted mantle (TDM) were estimated following Liew and Hofmann (1988). WPMB: Western belt, EPMB: Eastern belt. Data are the same as in Fig. 6.

mixing and mingling was reported from a subduction zone tectonic setting elsewhere in the world (e.g. Lachlan Fold Belt; Chappell and White, 1992). For instance, in the region of the central Andes, Eastern Puna, bimodal magmatism occurred in a subduction tectonic setting (e.g. Viramonte et al., 2007; Hauser et al., 2011; among others). Several geochemical features support (Figs. 6 and 8) the calc-alkaline nature of the igneous suite here studied, including the Eastern belt (~540-440 Ma; Viramonte et al., 2007; Hauser et al., 2011; Bahlburg et al., 2016 among others) and the Tastil batholith (~540-500 Ma; Hauser et al., 2011; Hongn et al., 2010 and references therein). However, the origin of Eastern Puna magmatic suit is a matter of current debate, particularly due to the peculiar geochemical features (high $FeO_t$-MgO-$K_2O$) and zircon ages inheritance patterns. Several petrogenetic models can be considered to evaluate the petrogenesis of the Eastern belt and Tastil batholith related magmatic rocks. Consequently, we evaluate the influence of previous processes proposed on the genesis and evolution of the studied rocks and those belonging to the Eastern belt and the Tastil batholith.

### *5.1. The role of magma mixing in the genesis of intermediate to acid magmas*

The studied intermediate to acid rocks comprise a range of intrusive types from tonalite to two-mica syenogranite. These granitoids and mafic igneous rocks, included hosted MME, form linear arrays with the major and trace elements (e.g. Cr, Th and V; Fig. 7). It is noted that some oxides and trace elements show more scatter variations both in mafic ($TiO_2$, $Al_2O_3$, Cr) and in acid members ($K_2O$, Ba, Rb). Linear compositional variations (Table 2), in combination with relatively limited scatter distributions, can be attributed to fractional crystallization, assimilation or mixing between two contrasting melts. Recent studies mainly focused on the CID, have demonstrated that the good covariation between major- and trace-elements against $SiO_2$ is mostly related to a magma mixing model (Suzaño et al., 2015). Comagmatic mafic components mingled and mixed with two mica-syenogranite in the CID and CBA, are well documented by field relationships. In a first approach, elemental distribution in most geochemical and isotopic (Nd) composition schemes of studied rocks and the Eastern belt and Tastil batholith units reveals a marked resemblance. This support that similar processes have acted in their petrogenesis. The inference is that chemical variations in granitic associations may result from the mixing process; based on the regular patterns displayed in elemental binary diagrams (Fig. 7).

In order to unambiguously distinguish between magma mixing, fractional crystallization and assimilation, we used the Microsoft Excel spreadsheet program of Ersoy and Helvaci (2010) and the set of partition coefficients for mafic magma compositions included therein. For geochemical modeling, we selected a monzogranite (sample 6/39, curve Mix1) and two mica-syenogranite (SD-15-01, curve Mix2) from the CID and two-mica syenogranite (D-14-5A) from CBA as representative of the granite that we assume is derived from partial melting of the older Puncoviscana Formation metamorphic high-grade equivalent. Acid end-members selected show a very similar composition as natural anatectic granitoids (Figs. 6 and 8) and they exhibit excellent mixing field relationships or hosted MME. For water-rich mafic end-member; we selected an MME (SD-17-07) and a dioritic body (CB-13-03) from CID and Amp-Qz-diorite (D-14-5B) from CBA. We use a dioritic body sample as Nd isotopic reservoir instead of MME since magma mixing can modify their Nd isotopic compositions significantly (Table A3).

Plagioclase, amphibole/clinopyroxene fractionation, and assimilation involving the local basement are evaluated in order to investigate its contribution to the genesis of intermediate to acid granitoids (Fig. 10a). Some mafic rock samples from the CBA and CID show moderate negative Eu anomalies (*Eu = 0.63–0.88) comparable with those of tonalities and granodiorites (*Eu = 0.55–0.76; Table A2, Fig. 8a, c). This suggests that some degree of fractional crystallization possibly contributed to their diverse compositions. However, our geochemical modeling reveals that fractional crystallization of a mafic magma involving the hypothetical fractionation of Amp/Cpx (Fig. 10a) and Pl (±10%; Fig. 10b) (which are characteristic of calc-alkaline systems) cannot explain the compositional variations in the trace elements. The Amp or Cpx fractionation can be excluded in our samples and from the Eastern belt and Tastil batholith granites, based on the lack of negative correlation of Gd/Yb with increasing La/Yb ratios (Fig. 10a). Moreover, with few exceptions, most samples from the CID, CBA, and other granites from Puna (Fig. 10b) are aligned along a curve predicted by the two-component mixing model instead of fractional crystallization of Pl and Amp/Cpx. We suggest that the observed linear variations in trace elements (Figs. 7 and 10) most likely resulted from homogeneously mixed melts.

Assimilation processes involving a large amount of eastern Puna basement (e.g. Viramonte et al., 2007; Bahlburg and Berndt, 2016) are also unlikely to explain the compositional variability of the studied samples. For instance, to explain the high MgO contents on intermediate rocks (Fig. 10c) is necessary more than 40% of assimilation (Bellos et al., 2015), which is hard to be accepted in petrological constrained terms. Most assimilation models (e.g., Reiners et al., 1995) assume that country rocks required heat of fusion, is derived from crystallization and cooling of the host magma. Assimilation suggests ratios of mass assimilated to mass crystallized on the order of 1 or even greater than 1, which is hard

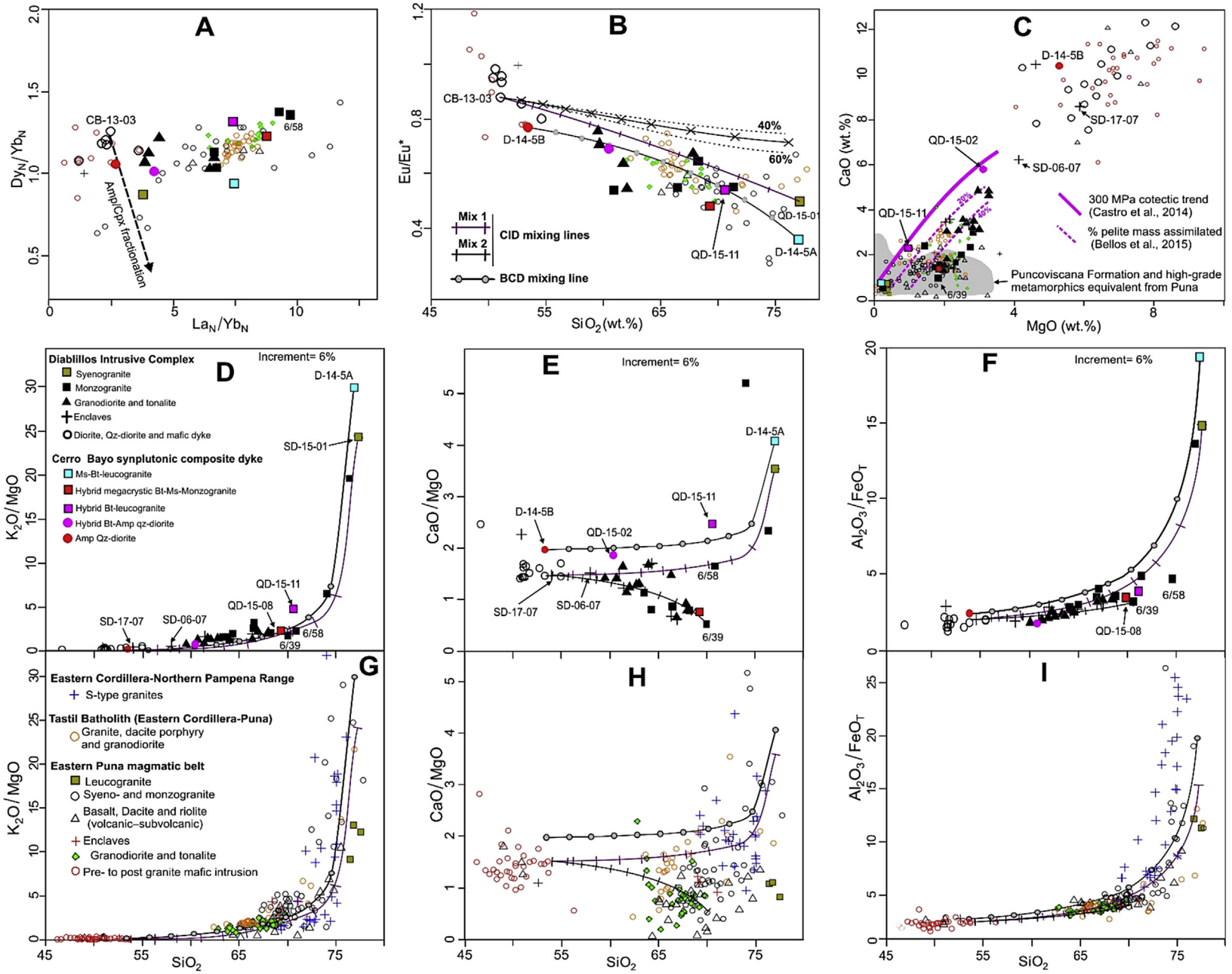


**Fig. 10.** Selected major and trace element variation diagrams to models the effect of mixing, fractional crystallization and assimilation processes. The mixing line computed for CID and CBA rocks are shown with EPMB, TB and crustal-derived granitoids for comparison. See text for choice of end-member composition. 50% Pl were assumed as fractionating phases for the fractional crystallization model. Tick marks on mixing and fractional crystallization lines are at 0.1 end-member fractions. See text for choice of end-member composition. (A) La/Yb vs. Dy/Yb. (B) Eu/Eu* vs. $SiO_2$, (C) MgO (wt.%) vs. CaO (wt.%). Dashed fractional crystallization arrays were calculated for 60% and 40% of Pl fractionation. (D) $K_2O$/MgO vs. SiO2 (wt.%), (E) CaO/MgO (wt.%) vs. $SiO_2$ (wt.%), (F) $Al_2O_3/FeO_T$ vs. $SiO_2$ (wt.%), (G), (H) and (I) are from EPMB, TB and crustal-derived melts. Data for the Puncoviscana Formation and high-grade metamorphic equivalent from Puna and Eastern Cordillera after Zimmermann (2005), Becchio et al. (1999) and Sola et al. (2013).

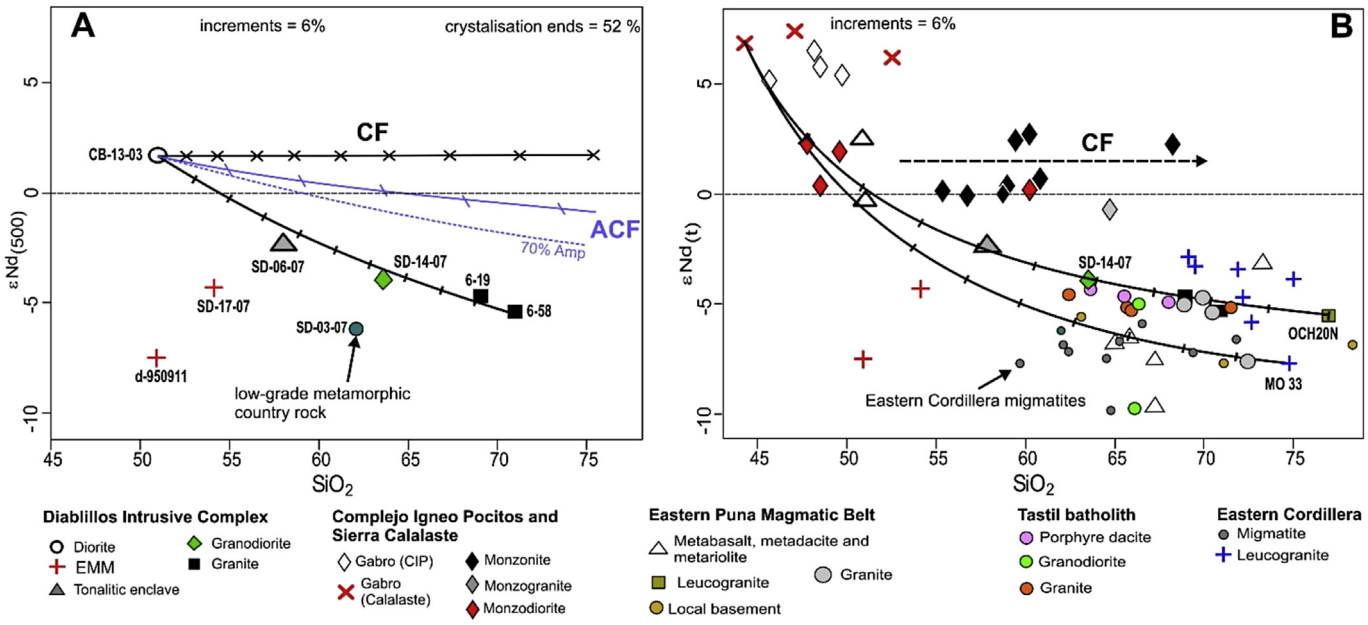


**Fig. 11.** Isotopic composition of rocks from CID and other granitoids from Puna and mafic rocks from the Western belt. (A) Variation $SiO_2$ (wt.%) vs. εNd(t) values for the granitoids from the CID. 50% Pl and 50% Amp and r = 0.5 were assumed as fractionating phases for the ACF model. Dashed ACF arrays were calculated for 70% of Amp fractionation. Symbols are the same as in Fig. 6 (B) Variation $SiO_2$ (wt.%) vs. εNd(t) for WPMB mafic rocks, EPMB, Tastil batholith and crustal-derived granites. The CID data are included in the figure inset for comparison. Data compiled after Damm et al. (1994); Becchio et al. (1999); Lucassen et al. (2001); Kleine et al. (2004); Viramonte et al. (2007); Hauser et al. (2011); Sola et al. (2013); Zimmermann et al. (2014) and this contribution.

**Table 2**
Computed magmatic suites correlation coefficient from Harker diagrams variations (Fig. 8). EPMB: Eastern belt.

| | $TiO_2$ | $Al_2O_3$ | FeOt | MgO | CaO | $Na_2O$ | $K_2O$ | $P_2O_5$ | Rb | V | Th | Cr |
|---|---|---|---|---|---|---|---|---|---|---|---|---|
| CBA | −1.0 | −0.93 | −0.89 | −0.98 | −0.96 | 0.73 | 1.00 | −0.86 | 0.93 | −0.99 | 0.96 | −0.48 |
| CID | −0.77 | −0.56 | −0.93 | −0.92 | −0.94 | 0.50 | 0.87 | −0.18 | 0.88 | −0.86 | 0.64 | −0.79 |
| EPMB | −0.74 | −0.56 | −0.95 | −0.95 | −0.94 | 0.88 | 0.88 | −0.19 | 0.55 | −0.91 | 0.40 | −0.56 |

to conceive if assimilation requires complete melting (Beard et al., 2005). On the other hand, isotopic systematics of Nd-Sr and inherited zircon in particular (e.g. Viramonte et al., 2007; Bahlburg and Berndt, 2016), provided evidence for the bulk assimilation of crustal xenoliths. However, Sola et al. (2013) showed the inherited zircons ages in the crustal-derived melt exhibit a large proportion of inherited zircon from the source (Puncoviscana Formation). Instead, most samples from CID, CBA coupled with the Eastern belt and Tastil batholith granites fall within the band predicted of a two-component mixing model (not shown). In addition, these granites departing from experimental cotectic trends (Castro, 2013; 2014) suggesting that granites do not represent liquids fractionated from an intermediate parental magma (no-cotectic trend; Suzaño et al., 2015).

Major ratios and isotopic data modeling (Fig. 10d–i) also, strongly suggests that mixing is the most likely process explaining the observed linear arrays in major and trace element compositions of the analyzed localities (Fig. 7). Langmuir et al. (1978) showed that on a ratio–element plot data consistent with mixing, it would lie along a hyperbolic curve between two contrasting end-members. In our study, these characteristic hyperbolic mixing arrays are observed for CID (Mix1 and Mix2 line) and CBA in plots for $K_2O$/MgO, CaO/MgO and $Al_2O_3/FeO_t$ vs. $SiO_2$ (Fig. 10d–g). Most intermediate-acid plutonic rocks fall into or close to the mix line predicted by different two-component mixing hypotheses. It suggests that each plutonic rock is a hybrid product due to the mixing in variable proportions between a mafic mantle-derived component and granites with crustal-derived melt affinities (Fig. 10d–f). Mixing test (Fourcade and Allegre, 1981) can be applied to estimate the proportion of mafic components needed to produce hybridized intermediate to acid magmas. As a test, an MME (SD-11-07, Table A2) and a two-mica syenogranite having high (SD-15-01) silica contents were chosen to perform the mixing calculation. In terms of major oxides, the proportion of mafic component 0.40–0.67 and 0.14–0.35 in the mixtures may produce the tonalite-granodiorites and monzogranites (linear correlations are greater than 0.93). The $K_2O$, MgO and $FeO_t$ major elements selected are critical for modeling because its high abundance in intermediate to acid compositions have led to formulate various petrogenetic models for the Eastern belt magmatism (see Fernández et al., 2008; Castro et al., 2009; Bellos et al., 2015).

Fig. 11 show comparison of the CID and CBA mixing lines and rocks from the Eastern belt and the Tastil batholith. Likewise to studied localities, linear (Fig. 7) and hyperbolic mixing arrays correlation (Fig. 10g–i) are also observed for all granites from the Eastern belt and the Tastil batholith. This array suggests that mixing processes likely occurred during the generation of these magmatic suites. In terms of major elements, the mafic and acid extremes of the Eastern belt could potentially represent regional end-members. According to the calculated mixing line, ca. 0.20 to 0.60 of mafic

component are required to produce the intermediate-acid magmas from the Eastern belt and the Tastil batholith.

In CBA, the field relationship indicates that successive acid pulses cut the previous mafic dyke and undergo progressive hybridization in dyke interiors (Fig. 3e). Hybrid leucogranites are featured by progressive variation of Bt (9–20%), Ms (disappear in hybrid ones) and Ttn (2.5–4.3%) modal proportion and enrichment in major elements such as $FeO_t$ (3.98 wt%), CaO (2.33 wt%), $TiO_2$ (0.72 wt%) and MgO (0.94 wt%) when are compared with Ms-bearing leucogranite end-member. We note that titanite is particularly an abundant accessory mineral in mafic end-member (5–8%) and probably it was incorporated (xenocryst) in leucogranites during mixing processes. Also, hybrid Bt-Qz-diorite from CBA and typical monzogranite from the Eastern belt shows the conversion of Amp to Bt and rapakivi texture respectively (Fig. 4). These textures are indicative of magma mixing environment. According to the mixing test (D-14-05A and D-14-05B were chosen for the calculation), 0.26–0.31 of the mafic component is required to produce the hybrid monzogranites (QD-15-11 and QD-15-08 samples) and 0.70 for the Bt-Qz-diorite.

Chemical and zoning pattern in Pl of tonalities, granodiorites, and monzogranites from CID recorded very well magma mixing processes. Pl grains from the most granites show core–An-rich mantle–outer rim structures in normal and reverse compositional zoning pattern. An values from two mica-monzogranite both increasing and decreasing from the core to mantle and then decreasing to the rim (Fig. 5a–c). Its Pl contain some cores with contrasting An content, Albite ($An_{6-9}$) and Andesine ($An_{46}$) that are indicative of the mafic and acid end-members acting in the mixture. Likewise, Pl phenocryst from granodiorite exhibit cores with $An_{33-52}$ and $An_{33-46}$, reverse zoning mantle from $An_{33-45}$ and then stabilized at $An_{30-34}$ (Fig. 5b). Pl phenocrysts and matrix lath-shape from tonalities show complexity zoning in core–mantle–rim or core-rim structures. Most core and mantle show reverse zoning (up to $An_{52}$ and $An_{51}$ respectively) and then decreasing to the outer rim in variable An content (Fig. 5c). Pl cores from tonalitic enclave show An contents compatible with these in mafic rocks. Such compositional changes in plagioclases from intermediate-acid magmas suggest that they underwent a new and calcic (An-rich mantles; hybrid environment) zone overgrowth and then re-equilibrated at the late crystallization stage after magma mixing (outer rim). The presence of plagioclases with An-rich cores suggest that they were mechanically transferred from injected mafic magma into the granitic magma. They show an An-rich core surrounded by a less calcic mantle zone related to the mixing process and An-poor outer rim compatible with intermediate-acid magmas composition. The plagioclases of mafic rocks (MME and intrusive body) show an inverse situation (Fig. 5d), that is, An-rich cores surrounded by an An-poor outer rim compatible with intermediate-acid magmas composition. Importantly, An-rich mantles and some cores of Pl phenocryst from intermediate to acid granites are comparable to those of the plagioclase cores from the mafic enclaves (Fig. 5). This implies that juvenile mafic melts, which served as a crucial component of the mafic enclaves, possibly made a significant contribution to the formation of these intermediate to acid granites (0.14–0.67 in the proportion of the mafic component in the mixture).

Correlations of Nd isotope with $SiO_2$ are useful in constraining the nature and extent mixing, fractionated crystallization and fractional crystallization-crustal assimilation in local shallow crustal levels (AFC; DePaolo, 1981) processes. Excellent negative correlation (except for the MME) between the whole-rock εNd(500 Ma) values and $SiO_2$ contents of the samples from CID (Fig. 11a) is observed. This variation favors that at least two kinds of magmas with contrasting Nd isotope compositions were mixed. In addition, hypothetical ACF and fractional crystallization computed lines from the mafic magma of CID involving local country rocks (Table A3) and the fractionation of Amp and Pl in variable proportions are not in agreement with the isotopic variation. Thus, more than 70% of Amp fractionation (showed as dashed line, Fig. 11a) is required to reproduce the isotopic variation in intermediate to acid rocks from the CID samples. This amount of fractionated Amp is not in agreement with the high MgO and FeOt contents observed in the intermediate to acid rocks from CID, On the other hand, two hypothetical mixing lines (Fig. 11b) were computed for Puna magmatic belt suites using a potential primitive mafic rock and two crustal-derived leucogranites from Puna (sample OCH20N; Viramonte et al., 2007) and Western Cordillera (sample MO 33, Sola et al., 2013). The great majority of the intermediate and silicic plutonic rocks from the Eastern belt (intrusive and volcanic equivalent rocks), Tastil batholith together with studied rocks appear close to the $SiO_2$ vs. εNd(t) hyperbolic array. This hypothesis is supported by mixing Sm–Nd model age for these granitoids (Fig. 9).

An increasing number of studies have shown that the Hf isotopic composition of zircon with crystallization ages is a powerful tool for elucidating the nature of magma sources and the role of magma mixing processes in the generation of granitoids (e.g. Belousova et al., 2006). Thus, available in situ zircon Hf isotopic data from the Eastern belt (~540–440 according with Hongn et al. (2010), Bahlburg et al. (2016)) and the Tastil batholith (541-500 Ma, Hauser et al., 2011; Hongn et al., 2010 and references therein) provide clear evidence for a contribution from juvenile parental mafic and crustal-derived magmas in their genesis. Granitoids and dacites porphyry from the Tastil batholith samples have relatively homogeneous εNd(t) showing crustal affinities (−4.4 to −9.8), but the zircon εHf(t) values ranging from−6.9 to +0.4 (Hauser et al., 2011). Zircons from the Eastern belt granites and volcanic equivalent are characterized by highly variable Hf isotopic compositions with εHf(t) values −16.0 to +3 (Hauser et al., 2011; Bahlburg et al., 2016) and show vertical array centered at ~500 Ma (Bahlburg et al., 2016). Thus, the wide range of zircon εHf(t) values from mafic to silico-intermediate rocks preclude a simple evolution via a closed-system fractionation. Thereby, εHf(t) values provide direct evidence (e.g. Belousova et al., 2006) for mixing between mafic and felsic magmas from different sources.

### 5.2. Petrogenesis of the mafic rocks and related MME

According to our study, the MME in the granites from the CID and CBA are generated through both injections of a mafic/acid magmatic component into a granitic magma chamber (e.g. Vernon, 1984) or an early mafic dyke (e.g. Collins et al., 2000; synplutonic composite dyke) via a mixing/mingling process. Several lines of evidence lead us to conclude that the MME were generated via these mechanisms or a combination of them (Barbarin, 2005). Firstly, abundant petrological observations such as enclaves with ellipsoidal–ovoidal shapes, transitional zones in the contacts, multi-component enclaves (Fig. 3b–f), and xenocrysts exchanges within the more diffused enclaves (Fig. 5a) are consistent with the MME from the CID and CBA representing globules of near-liquidus hybridized mafic melt. These features are particularly common in the hybrid magma system (e.g. Hibbard, 1995; Barbarin and Didier, 1992). Hence, it is probably that enclaves represent hybrid magmas.

In the particular case of CBA, field relationships indicate in-situ MME generation and progressive leucogranites hybridization through the injection into the early mafic dyke by at least two synmagmatic pulses of acid material (Fig. 3c–f). Furthermore, MME of the CID and CBA have igneous mineralogy and textures with feldspar xenocrysts and disequilibrium features such as resorbed

surface and zoning in Pl, rapakivi texture, quartz ocelli and acicular apatite (Fig. 4). All these textures are interpreted as reflecting physic-chemical and/or thermal changes in the melt during crystal growth (e.g. Vernon, 1984; Pietranik and Koepke, 2014). Mineral chemistry further supports magma mixing, particularly the abundance of core-mantle-rim structures in Pl and biotite composition in all facies from the CID (Fig. 5, Fig. A1). The negative correlation trend of the biotite from enclaves and host rocks on the $FeO_t$ vs. MgO diagrams (supplementary Fig. A1) can be explained by continuous Fe–Mg exchange during magma mixing phenomena. The rims of Pl in the MME, including those from Qz-diorite bodies (Fig. 5d) are identical in An content ($An_{28-30}$) to the Pl in the felsic host rocks, whereas, the cores and mantle are more calcic ($An_{41-60}$). In addition, some Pl grains from the felsic host rocks have calcium-rich cores ($An_{46}$), which are overgrown by sodium-rich rim ($An_{28-30}$) (Fig. 5a, f). Crystallization in a closed magma system or country-rock assimilation cannot account for such kind of abrupt compositional discontinuities. Instead, this relationship is interpreted as the result of mixing magmas. Preservation of the compositional and textural disequilibrium features in the Pl suggests rapid crystallization at shallow depth emplacement.

The MME and host granites have identical Nd isotopic compositions (Fig. 9, Table A3). This could be attributed to the rapid diffusive isotopic equilibrium after entrainment (e.g. Elburg, 1996), although dioritic intrusive body yields εNd(500 Ma) +1.7 (Table A3). However, we note that the MME and mafic bodies from the CID have almost identical P-T conditions of crystallization. This noticeable difference in Nd isotopes and the similar P-T condition can be used to distinguish the magma mixing and autolith hypotheses.

The Sr-Nd isotope compositions indicate the contribution of the mantle and crustal sources to the generation of the mafic magmas from the CID and other mafic rocks along the Western- and Eastern belt (Fig. 9). The nature of the juvenile igneous component is constrained by the lowest initial $^{87}Sr/^{86}Sr$ ratio and the high εNd(t) values (Kleine et al., 2004; Viramonte et al., 2007; Hauser et al., 2011; Zimmermann et al., 2014). However, as pointed out previously, magma mixing and assimilation can significantly modify the chemistry of mafic magmas (e.g. Barbarin, 2005). Thus, the primary whole-rock Sr/Nd isotopic signatures of the mafic magma (MME) may have been partially or almost entirely overprinted.

Relatively high MgO (<8.6 wt%), $FeO_t$ (<15.6 wt%), CaO (<12.3 wt %), moderate Co (<70 ppm), Cr (<444 ppm and CBA = 30–40 ppm), Y (<62 ppm) contents characterized the mafic rocks from the CID and CBA. These values are consistent with the Eastern belt mafic rocks but are lower than a primary or primitive basaltic magma derived from a mantle peridotite source (e.g. Wilson, 1989). This suggests that at least some early fractionation process could be involved in the first stages of evolution of mafic rocks. Mafic rocks also have low Nb/U (4.67–10.3) and Ce/Pb (13.2–32.0) ratios, which are partially similar to those of continental crust (Nb/U = 6.2 and Ce/Pb = 3.9; Rudnick and Fountain, 1995) and those of mid-ocean ridge and oceanic island arc basalts (MORB and OIB; Nb/U = 47 ± 10 and Ce/Pb = 25 ± 5; Hofmann et al., 1986). Mafic rocks are enriched in LILE and depleted in HFSE (e.g. Fig. 8b, d). Their REE pattern shows flat to moderate enrichment in LREE (Fig. 8a, c) and little fractionated HREE without fractionation of the middle REE relative to the HREE (melting of a source lacking in garnet, e.g. Manikyamba et al., 2014). These trace element features coupled with Sr-Nd isotope compositions suggest an enriched subcontinental lithospheric mantle source. However, the effect of early crustal contamination and fractionation (e.g. Kleine et al., 2004) during the evolution of the entire Puna mafic magmatism also needs to be considered.

### 5.3. Estimation of pressure, temperature and water-in-melt

The total Al contents in amphiboles largely rely on the pressure when they crystallized (e.g. Schmidt, 1992). Aluminum-in-hornblende geobarometers (Table A1) over seven Hbl–Pl pairs were used to estimate the pressures under which the MMEs and Qz-diorites intrusive bodies formed. In addition, we use the Hbl-Pl thermometer to calculate the crystallization temperatures of the CID mafic rocks. Based on these calculations, the MME and Qz-diorites bodies crystallized under the similar P-T conditions (Table A1). The pressures calculated from the geobarometer of Schmidt (1992) (average 2.34–2.48 kbar) and Anderson and Smith (1995) (average 2.21–2.48 kbar) correspond to shallow depths of ~8–9 km (assuming that 1 kbar is equivalent to ca. 3.5 km of the crust). Using the thermometers of Holland and Blundy (1994), the calculated equilibrium temperature of the co-existing Hbl–Pl pair in the MME (677–692 °C, average = 684 °C) is lower than the most common values calculated in the Qz-diorite body (726–727 °C; Table A1). The obtained pressures and temperatures possibly represent the final emplacement conditions.

Ridolfi et al. (2010) proposed an empirical formula to estimate the $H_2O$ content dissolved in magmas solely based on the compositions of crystallized amphiboles (error of ca. 15%). The method was calibrated for volcanic rocks in order to reconstructs pre-eruptive conditions of amphibole-bearing calc-alkaline magmas in the upper-mid crust settings of continental volcanoes (<40 km, ca. <10 kbar) (e.g. da Cunha et al., 2016). Calculation shows that the Qz-diorites intrusive bodies yield water contents of 4.37–5.91 wt% (Table A1). Qz-diorites and MME are dominated by Amp (Fig. 4c) and their stability largely relies on the $H_2O$ content in the magma (e.g. Ridolfi et al., 2010).

### 5.4. Integrated model of magmatic processes

There is a generalized consensus that Puna Early Paleozoic calco-alkaline magmatism along the western border of Gondwana formed in an east-dipping active continental margin setting (e.g. Rapela et al., 1998; Kleine et al., 2004) due to subduction of the palaeo-Pacific plate without accretion of various exotic or para-uthochthonous terrane (e.g. Lucassen and Franz, 2005; Lucassen et al., 2000).

Magmatic ages are broadly the same (~540-440 Ma) and overlapped in space during the evolution of the arc system (e.g. Coira et al., 1999; Lucassen et al., 2000) from the Eastern Cordillera (Hauser et al., 2011; Hongn et al., 2010 and references therein) through the Eastern Puna (e.g. Viramonte et al., 2007; Suzaño et al., 2015; Bahlburg et al., 2016) to the Western magmatic belt (Kleine et al., 2004; Escayola et al., 2011; Zimmermann et al., 2014). It suggests a long-lasting continental margin dominated by subduction with the formation of a widespread magmatic activity at least on the ~540-440 Ma. This widespread magmatic activity including contemporaneous mafic and dominate peraluminous acid magmatic activity (e.g. Becchio et al., 1999). For a wide distribution of a long-lasting magmatic activity, it is necessary that this magmatism develops in a backarc environment such as proposed by Hyndman et al. (2005) where the high heat flow is independent of compression or extension setting.

Many intrusive intermediate-acid granitoids contain abundant enclaves (intermediate to MME, Bahlburg, 1990; Poma et al., 2004; Viramonte et al., 2007; Suzaño et al., 2015; among others) and are intruded by few stocks of mafic composition and synplutonic-to late mafic dykes. The shape and size of the MME indicate contemporaneous flow and mixing or mingling of partly molten felsic-mafic magmas at the emplacement level (e.g. synplutonic composite dyke from CBA). However, although many intrusive

granite bodies contain intermediate to mafic enclaves, with some exceptions, most of them are homogeneous without obvious evidence of macroscopic disequilibrium textures. On the other hand, we systematically show that both mafic and intermediate-acid magmatism from CID, CBA, and along the Puna magmatic rocks (including volcanic ones) and Tastil batholith, exhibit very similar trace, major and isotopic (Sr-Nd-Hf) composition and geochemical behavior in several variation schemes (Figs. 6–11). Thus, accepting the mixing model for the genesis of the CID and CBA intermediate-acid granites, their geochemical and isotopic composition can be used to place further constraints on the magmas driven by magma mixing. Thereby, the fact that the studied rocks and the Eastern belt and Tastil batholith show a marked resemblance, it could be argued accordingly that those rocks were generated mainly by magma mixing process. This implies that the processes related to magma mixing was regionally extended and have operated at least from 540 to 440 Ma in a long-lasting active continental margin environment (e.g. Lucassen et al., 2000). According to our model, acid magmas contain a significant amount (up to 35%) of mafic magma. The widespread regional distribution of acid rocks suggests a significant volume of mafic magma that has not been considered before in the literature.

We suggest that the main mixing event occurred in deep-seated magma chambers (e.g. Annen and Sparks, 2002) where hydrous mafic sills or laccoliths were emplaced into the middle-lower crust and triggered partial melting of fertile metasediments. A similar interpretation is proposed in the Sierra Valle Fértil magmatism (e.g. Otamendi et al., 2009). The mayor, trace element and isotope record of Puna magmatism (e.g. Lucassen et al., 2000) suggest that continental basement is a significant component; hence, modification of mafic and acid melts must have taken place in the middle to deeper crust beneath the arcs. This scenario allows us to propose a deep crustal domain of primary melt modification (Kleine et al., 2004) known as the zone of melt mixing, assimilation, storage, and homogenization (MASH, Hildreth and Moorbath, 1988).

Along the southwestern border of Gondwana, underplating of the crust by mantle-derived mafic magmas has been regarded as important heat source factors in the metamorphism (HT/LP, Lucassen et al., 2000) and origins of the widespread Lower Paleozoic granitoids (e.g. Grissom et al., 1998; Lucassen et al., 2000; Hongn et al., 2014). Extensive and variable interaction degree between the crustal-derived- and juvenile mafic melts may have produced large bodies of hybrid magmas (monzogranite to Qz-diorite) at depth level crust. Scarce leucogranites from Puna represent pure crustal-derived felsic melts since they have very similar compositions at normal degrees of partial melting over a large source region (Figs. 9–11) of metasedimentary rocks of the Puncoviscana sequence (e.g. Sola et al., 2013).

The produced hybrid intermediate to acid melts then, were emplaced as plutons in the upper crust level (~8–9 km) as determined for the CID granitoids. In some cases, injection of successive pulses of mafic magma into ascending magma would have resulted in the formation of MME (Fernández and Barbarin, 1991). Multi-component enclave occurrences support succession and repetition of the various exchange (chemical and physical) processes, and constant evolution of the end-members affected by these processes (Barbarin and Didier, 1992). The MME can be plausibly explained in terms of direct fractionation of an underplating mafic precursor. More probably, mafic rocks underwent early assimilation (e.g. Kleine et al., 2004; Otamendi et al., 2012) and hybridization with small amounts of felsic melts according to the field, petrographic and isotopic composition constraint. A range of styles and mechanisms of mixing and mingling such as bulk physical mixing, physical exchanges, diffusion, crystallization, and disaggregation are proposed to account for the diversity of textural, morphology, contact types and geochemical relationships between the enclaves and the host granite (Fig. 3). At upper crustal levels, some of these granitic plutons were injected by successive pulses of mafic magmas resulting in the formation dismembered synplutonic and late mafic dykes.

We note that in the CBA, injection of successive pulses of two-mica syenogranite (crustal-derived melt) magma into the early mafic dyke produce at least two stages of hybridization by the interaction of felsic with mafic melt (interpreted as composite synplutonic dyke). The petrography and geochemistry of the hybrid Bt-Ttn monzogranites from CBA illustrate a number of features, which are compatible with magma mixing. This could be alternative of hybridization mechanism (e.g. Collins et al., 2000) that produces high $SiO_2$ (70.6 wt%), $FeO_t$ (3.98 wt%), $K_2O$ (4.43 wt%) and moderate MgO (0.94 wt%) contents, which are very similar to the typical Eastern belt and Tastil batholith granites. In addition, intermediate-acid granitoids (tonalite to monzogranite) from the Eastern Puna and Tastil batholith granitoids show distinctive geochemical features respect to typical Cordilleran-type batholith (e.g. the Mesozoic–Cenozoic cordilleran-type batholiths: e.g. Sierra Nevada batholith, Lee et al., 2007). Thus, Puna magmatism (average n = 180; $SiO_2$ = 68.63 wt%) show high $FeO_t$ (4.45 wt%) and MgO (1.66 wt%) for low CaO (1.85 wt%), $Na_2O$ (2.93 wt%) in combination with the high $K_2O$ (3.84 wt%) contents. In general, peninsular batholiths (average n = 197; $SiO_2$ = 68.31 wt%) show lower $FeO_t$ (3.33 wt%), MgO (1.29 wt%), $K_2O$ (2.64 wt%) and higher CaO (3.44 wt %), $Na_2O$ (3.57 wt%) than Puna magmatism. Geochemical features of the Cordilleran-type batholith resulted by a dominant process related to fractionation of a parental andesitic magma (e.g. Sisson et al., 2005) following an experimental cotectic trend (Castro, 2013). In contrast, the whole-rock compositions from the CID and the Eastern belt and Tastil batholith reflect no-cotectic trend (Suzaño et al., 2015) suggesting a minor effect of magmatic fractionation from a parental mafic magma.

## 6. Conclusions

Field and petrological observations together with elemental and isotopic composition reveal that diorites, Qz-diorites, tonalities, granodiorites, monzogranites and leucogranites from the CID and CBA form a continuous trend produced by mixing between hydrous juvenile mantle- and crustal-derived magmas with a minor effect of fractional crystallization and local assimilation processes.

The two-mica syenogranites were predominantly derived from anatexis of crustal materials broadly represented by Puncoviscana Formation due to underplating of hydrous juvenile mafic magmas. Subsequent variable degree of mixing of crust-derived melts with the mafic melts proportion was possibly responsible for the geochemical diversity of the granitoids intruded in the upper crust. According to the mixing test, the proportion of mafic component 0.40–0.67 and 0.14–0.35 are required to explain the major and trace element composition of tonalite-granodiorites and monzogranites. The mafic and tonalitic-granodioritic enclaves within the plutons of CID granitoids and synplutonic composite dike from Cerro Bayo area are interpreted to be igneous in origin and represent coeval magmatic globules commingled with their host magmas.

Geochemistry and isotopes of the intermediate to acid granites from the Eastern belt and the Tastil batholith may well represent the hybrid magmas. According to the mixing model, ca. 0.20 to 0.60 of mafic component are required to produce these granites. This implies that the processes related to magma mixing identified in the CID and CBA was regional, volumetrically significant and plays a critical role in the origin and evolution of these rocks. Thus, the mafic and acid extremes of the Puna magmatic belts could

potentially represent regional end-members.

## Acknowledgments

We thank Hugo Delgados (Laboratorio de Petrología, UNAM) for help with electron microprobe analyses and Laboratorio de petrotomía INENCO-CONICET for thin section elaboration. This study was financially supported by the Research Project of the CIUNSa (1978/0 and 2314) and CONICET (D4247). The support and hospitality of both Silver standard and Rodinia Lithium are gratefully acknowledged. We are grateful to Drs. Juan Otamendi and Alina Tibaldi reviewers for their constructive criticisms that significantly improved the manuscript. Special thanks to editor Dr. V. Ramos for his diligence.

## Appendix A. Supplementary data

Supplementary data related to this article can be found at http://dx.doi.org/10.1016/j.jsames.2017.02.008.

## References

Abdel-Rahman, A.F.M., 1994. Nature of biotites from alkaline, calc-alkaline, and peraluminous magmas. J. Petrol. 35, 525–541.
Anderson, J., Smith, D., 1995. The effects of temperature and $f_{O2}$ on the Al-in-hornblende barometer. Am. Mineral. 80, 549–559.
Annen, C., Sparks, R.S.J., 2002. Effects of repetitive emplacement of basaltic intrusions on thermal evolution and melt generation in the crust. Earth Planet. Sci. Lett. 203, 937–955.
Bahlburg, H., 1990. The Ordovician basin in the Puna of NW Argentina and N Chile: geodynamic evolution from back-arc to foreland basin. Geotekt. Forschungen 75, 1–107.
Bahlburg, H., Berndt, J., 2016. Provenance from zircon U-Pb age distributions in crustally contaminated granitoids. Sediment. Geol. 336, 161–170.
Bahlburg, H., Berndt, J., Gerdes, A., 2016. The ages and tectonic setting of the Faja Eruptiva de la Puna Oriental, Ordovician, NW Argentina. Lithos 256–257, 41–54.
Barbarin, B., 2005. Mafic magmatic enclaves and mafic rocks associated with some granitoids of the central Sierra Nevada batholith, California: nature, origin, and relations with the hosts. Lithos 80, 155–177.
Barbarin, B., Didier, J., 1992. Genesis and evolution of mafic microgranular enclaves through various types of interaction between coexisting felsic and mafic magmas. Trans. R. Soc. Edinb. Earth Sci. 83, 145–153.
Beard, J.S., Ragland, P.C., Crawford, M.L., 2005. Reactive bulk assimilation: a model for crust-mantle mixing in silicic magmas. Geology 33, 681–684.
Becchio, R., Lucassen, F., Franz, G., Viramonte, J., 1999. El basamento paleozoico inferior del noroeste de Argentina (23–27 S)—metamorfismo y geocronologia. In: González Bonorino, G., Omarini, J.V., R. (Eds.), Geología del Noroeste Argentino. XIV Congreso Geológico Argentino, Salta, Argentina, pp. 58–72.
Bellos, L.I., Castro, A., Díaz-Alvarado, J., Toselli, A., 2015. Multi-pulse cotectic evolution and in-situ fractionation of calc-alkaline tonalite-granodiorite rocks, Sierra de Velasco batholith, Famatinian belt, Argentina. Gondwana Res. 27, 258–280.
Belousova, E.A., Griffin, W.L., O'Reilly, S.Y., 2006. Zircon crystal morphology, trace element signatures and Hf isotope composition as a tool for oetrogenetic modelling: examples from Eastern Australian granitoids. J. Pet. 47, 329–353.
Bock, B., Bahlburg, H., Wörner, G., Zimmermann, U., 2000. Tracing crustal evolution in the southern central Andes from late precambrian to permian with geochemical and Nd and Pb isotope data. J. Geol. 108, 515–535.
Büttner, S.H., Glodny, J., Lucassen, F., Wemmer, K., Erdmann, S., Handler, R., Franz, G., 2005. Ordovician metamorphism and plutonism in the Sierra de Quilmes metamorphic complex: implications for the tectonic setting of the northern Sierras Pampeanas (NW Argentina). Lithos 83, 143–181.
Castro, A., 2013. Tonalite–granodiorite suites as cotectic systems: a review of experimental studies with applications to granitoid petrogenesis. Earth-Science Rev. 124, 68–95.
Castro, A., Díaz-Alvarado, J., Fernández, C., 2014. Fractionation and incipient self-granulitization during deep-crust emplacement of Lower Ordovician Valle Fértil batholith at the Gondwana active margin of South America. Gondwana Res. 25, 685–706.
Castro, A., García-Casco, A., Fernández, C., Corretgé, L.G., Moreno-Ventas, I., Gerya, T., Löw, I., 2009. Ordovician ferrosilicic magmas: experimental evidence for ultrahigh temperatures affecting a metagreywacke source. Gondwana Res. 16, 622–632.
Chappell, B.W., White, A.J.R., 2001. Two contrasting granite types: 25 years later. Aust. J. Earth Sci. 48, 489–500.
Chappell, B.W., White, A.J.R., 1992. I- and S-type granites in the Lachlan Fold belt. In: Geological Society of America Special Papers. Geological Society of America, pp. 1–26.
Coira, B., Koukharsky, M., Guevara, S.R., Cisterna, C.E., 2009. Puna (Argentina) and northern Chile Ordovician basic magmatism: a contribution to the tectonic setting. J. South Am. Earth Sci. 27, 24–35.
Coira, B., Perez, B., Flores, P., Kay, S.M., Woll, B., Hanning, M., 1999. Magmatic sources and tectonic setting of Gondwana margin Ordovician magmas, northern Puna of Argentina and Chile. Spec. Pap. - Geol. Soc. Am. 336, 145–170.
Collins, W.J., Richards, S.R., Healy, B.E., Ellison, P.I., 2000. Origin of heterogeneous mafic enclaves by two-stage hybridisation in magma conduits (dykes) below and in granitic magma chambers. Earth Environ. Sci. Trans. R. Soc. Edinb. 91, 27–45.
da Cunha, I.R.V., Dall'Agnol, R., Feio, G.R.L., 2016. Mineral chemistry and magnetic petrology of the archean planalto suite, carajás province–amazonian craton: implications for the evolution of ferroan archean granites. J. South Am. Earth Sci. 67, 100–121.
Damm, K., Harmon, R.S., Kelley, S., 1994. Some isotopic and geochemical constraints on the origin and evolution of the central andean basement (19°-24°S). In: Reutter, K.-J., et al. (Eds.), Tectonics of the Southern Central Andes, pp. 263–276.
Damm, K.-W., Pichowiak, S., Harmon, R.S., Todt, W., Kelley, S., Omarini, R., Niemeyer, H., 1990. Pre-Mesozoic evolution of the central Andes; the basement revisited. In: Geological Society of America Special Papers. Geological Society of America, pp. 101–126.
DePaolo, D., 1981. A neodymium and strontium isotopic study of the Mesozoic calc-alkaline granitic batholiths of the Sierra Nevada and Peninsular Ranges, California. J. Geophys. Res. 86, 10470–10488.
Didier, J., 1973. Granites and Their Enclaves: the Bearing of Enclaves on the Origin of Granites, Developments in Petrology. Elsevier, Amsterdam, p. 254.
Douce, A.E.P., Harris, N., 1998. Experimental constraints on Himalayan anatexis. J. Petrol. 39 (4), 689–710.
Ducea, M.N., Otamendi, J.E., Bergantz, G.W., Jianu, D., Petrescu, L., 2015. The ordovician Famatinian-Puna arc. GSA Mem. 212, 125–138.
Elburg, M.A., 1996. Evidence: of isotopic equilibration between microgranitoid enclaves and host granodiorite, Warburton Granodiorite, Lachlan Fold Belt, Australia. Lithos 38, 1–22.
Ersoy, Y., Helvaci, C., 2010. FC-AFC-FCA and mixing modeler: a Microsoft Excel spreadsheet program for modeling geochemical differentiation of magma by crystal fractionation, crustal assimilation and mixing. Comput. Geosci. 36, 383–390.
Escayola, M.P., van Staal, C.R., Davis, W.J., 2011. The age and tectonic setting of the Puncoviscana Formation in northwestern Argentina: an accretionary complex related to Early Cambrian closure of the Puncoviscana Ocean and accretion of the Arequipa-Antofalla block. J. South Am. Earth Sci. 32, 438–459.
Fernández, A.N., Barbarin, B., 1991. Relative rheology of coeval mafic and felsic magmas: nature of resulting interaction processes and shape and mineral fabrics of mafic microgranular enclaves. In: Didier, J., Barbarin, B. (Eds.), Enclaves and Granite Petrology. Elsevier, Amsterdam, pp. 263–276.
Fernández, C., Becchio, R., Castro, A., Viramonte, J.M., Moreno-Ventas, I., Corretgé, L.G., 2008. Massive generation of atypical ferrosilicic magmas along the Gondwana active margin: implications for cold plumes and back-arc magma generation. Gondwana Res. 14, 451–473.
Fourcade, S., Allegre, C.J., 1981. Trace elements behavior in granite genesis: A case study the calc-alkaline plutonic association from the querigut complex (Pyrénées, France). Contrib. Mineral. Petrol. 76 (2), 177–195.
Frost, B.R., Frost, C.D., 2008. A geochemical classification for feldspathic igneous rocks. J. Pet. 49, 1955–1969.
Grissom, G.C., Debari, S.M., Snee, L.W., 1998. Geology of the Sierra de Fiambalá, Northwestern Argentina: implications for Early Palaeozoic Andean tectonics. Geol. Soc. Lond. Spec. Publ. 142, 297–323.
Hauser, N., Matteini, M., Omarini, R.H., Pimentel, M.M., 2011. Combined U-Pb and Lu-Hf isotope data on turbidites of the Paleozoic basement of NW Argentina and petrology of associated igneous rocks: implications for the tectonic evolution of western Gondwana between 560 and 460Ma. Gondwana Res. 19, 100–127.
Hibbard, M.J., 1995. Petrography to Petrogenesis.Pdf. Prentice Hall, New Jersey, p. 587.
Hildreth, W., Moorbath, S., 1988. Crustal contributions to arc magmatism in the Andes of central Chile. Contrib. to Mineral. Pet 98 (4), 455–489.
Hofmann, A.W., Jochum, K.P., Seufert, M., White, W.M., 1986. Nb and Pb in oceanic basalts: new constraints on mantle evolution. Earth Planet. Sci. Lett. 79, 33–45.
Holland, T., Blundy, J., 1994. Non-ideal interactions in calcic amphiboles and their bearing on amphibole–plagioclase thermometry. Contrib. Mineral. Petrol. 116, 433–447.
Hongn, F.D., Seggiaro, R.E., 2001. Hoja Geológica 2566-III, Cachi, Servicio Geológico Minero Argentino, Boletín 248. Buenos Aires, Scale 1: 250,000.
Hongn, F.D., Tubía, J.M., Aranguren, A., Vegas, N., Mon, R., Dunning, G.R., 2010. Magmatism coeval with lower Paleozoic shelf basins in NW-Argentina (Tastil batholith): constraints on current stratigraphic and tectonic interpretations. J. South Am. Earth Sci. 29, 289–305.
Hongn, F.D., Tubía, J.M., Esteban, J.J., Aranguren, A., Vegas, N., Sergeev, S., Larionov, A., Basei, M., 2014. The Sierra de Cachi (Salta, NW Argentina): geological evidence about a Famatinian retro-arc at mid crustal levels. J. Iber. Geol. 40, 225–240.
Hyndman, R.D., Currie, C.A., Mazzotti, S.P., 2005. Subduction zone backarcs, mobile belts, and orogenic heat. GSA Today 15 (2), 4–10.
Insel, N., Grove, M., Haschke, M., Barnes, J.B., Schmitt, A.K., Strecker, M.R., 2012.

Paleozoic to early Cenozoic cooling and exhumation of the basement underlying the eastern Puna plateau margin prior to plateau growth. Tectonics 31, 6.
Kirschbaum, A., Hongn, F., Menegatti, N., 2006. The Cobres plutonic complex, eastern Puna (NW Argentina): petrological and structural constraints for lower paleozoic magmatism. J. South Am. Earth Sci. 21, 252–266.
Kleine, T., Mezger, K., Zimmermann, U., Münker, C., Bahlburg, H., 2004. Crustal evolution along the early ordovician proto-andean margin of Gondwana: trace element and isotope evidence from the complejo igneo Pocitos (northwest Argentina). J. Geol. 112, 503–520.
Langmuir, C.H., Vocke, R.D., Hanson, G.N., Hart, S.R., 1978. A general mixing equation with applications to Icelandic basalts. Earth Planet. Sci. Lett. 37, 380–392.
Leake, B.E., Woolley, A.R., Arps, C.E., Birch, W.D., Gilbert, M.C., Grice, J.D., Linthout, K., 1997. Nomenclature of amphiboles: Report of the subcommittee on amphiboles of the International Mineralogical Association Commission on new minerals and mineral names. Mineral. Mag. 61 (2), 295–321.
Lee, C.-T.A., Morton, D.M., Kistler, R.W., Baird, A.K., 2007. Petrology and tectonics of Phanerozoic continent formation: from island arcs to accretion and continental arc magmatism. Earth Planet. Sci. Lett. 263, 370–387.
Liew, T.C., Hofmann, A.W., 1988. Precambrian crustal components, plutonic associations, plate environment of the Hercynian Fold Belt of central Europe: Indications from a Nd and Sr isotopic study. Contrib. Mineral. Petrol 98, 129–138.
Loewy, S.L., Connelly, J.N., Dalziel, I.W.D., 2004. An orphaned basement block: the Arequipa-Antofalla Basement of the central Andean margin of South America. Geol. Soc. Am. Bull. 116 (1–2), 171–187.
López, J.F., Quiroga, M.F., Suzaño, N., Becchio, R., Ortiz, A., Arnosio, M., 2016. Magmatismo silíceo y niveles de emplazamiento durante el paleozoico inferior en el área de tajamar-quebradas de agua de Castilla y Cajón, Salta. Rev. la Asoc. Geol. Argent. 73 (3), 348–368.
Lucassen, F., Becchio, R., 2003. Timing of high-grade metamorphism: early Palaeozoic U-Pb formation ages of titanite indicate long-standing high-T conditions at the western margin of Gondwana (Argentina, 26-29°S). J. Metamorph. Geol. 21, 649–662.
Lucassen, F., Becchio, R., Franz, G., 2011. The early Palaeozoic high-grade metamorphism at the active continental margin of West Gondwana in the Andes (NW Argentina/N Chile). Int. J. Earth Sci. 100, 445–463.
Lucassen, F., Becchio, R., Harmon, R., Kasemann, S., Franz, G., Trumbull, R., Wilke, H.G., Romer, R.L., Dulski, P., 2001. Composition and density model of the continental crust at an active continental margin - the Central Andes between 21° and 27°S. Tectonophysics 341, 195–223.
Lucassen, F., Becchio, R., Wilke, H.G., Franz, G., Thirlwall, M.F., Viramonte, J., Wemmer, K., 2000. Proterozoic ± paleozoic development of the basement of the central Andes ( 18 ± 26 8 S );a mobile belt of the south american craton. J. South Am. Earth Sci. 13, 697–715.
Lucassen, F., Franz, G., 2005. The early palaeozoic orogen in the central Andes: a non-collisional orogen comparable to the cenozoic high plateau?, in: terrane processes at the margins of Gondwana. Geol. Soc. Lond. 257–273.
Manikyamba, C., Saha, A., Santosh, M., Ganguly, S., Rajanikanta Singh, M., Subba Rao, D.V., Lingadevaru, M., 2014. Neoarchaean felsic volcanic rocks from the Shimoga greenstone belt, Dharwar Craton, India: geochemical fingerprints of crustal growth at an active continental margin. Precambrian Res. 252, 1–21.
Méndez, V., 1972. Faja eruptiva de la Puna oriental. 5° Congr. Geol. Argent. 4, 89–100.
Nakamura, N., 1974. Determination of REE, Ba, Fe, Mg, Na and K in carbonaceous and ordinary chondrites. Geochim. Cosmochim. Acta 38, 757–775.
Otamendi, J.E., Ducea, M.N., Bergantz, G.W., 2012. Geological, petrological and geochemical evidence for progressive construction of an Arc crustal Section, Sierra de Valle Fértil, Famatinian Arc, Argentina. J. Pet. 53, 761–800.
Otamendi, J.E., Ducea, M.N., Tibaldi, A.M., Bergantz, G.W., de la Rosa, J.D., Vujovich, G.I., 2009. Generation of tonalitic and dioritic magmas by coupled partial melting of gabbroic and metasedimentary rocks within the deep crust of the Famatinian magmatic arc, Argentina. J. Pet. 50, 841–873.
Otamendi, J.E., Pinotti, L.P., Basei, M.A.S., Tibaldi, A.M., 2010. Evaluation of petrogenetic models for intermediate and silicic plutonic rocks from the Sierra de Valle Fértil-La Huerta, Argentina: petrologic constraints on the origin of igneous rocks in the Ordovician Famatinian-Puna paleoarc. J. South Am. Earth Sci. 30, 29–45.
Palma, M.A., Parica, P.D., Ramos, V.A., 1986. El granito de Archibarca: su edad y significado tectonico, provincia de Catamarca. Rev. la Asoc. Geol. Argent. 41, 414–419.
Pankhurst, R.J., Rapela, C.W., Fanning, C.M., 2000. Age and origin of coeval TTG, I- and S-type granites in the famatinian belt of NW Argentina. Spec. Pap. 350 fourth hutt. Symp. Orig. Granites relat. Rocks 350, 151–168.
Pankhurst, R.J., Rapela, C.W., Saavedra, J., Baldo, E., Dahlquist, J., Pascua, I., Fanning, C.M., 1998. The Famatinian magmatic arc in the central Sierras Pampeanas: an Early to Mid-Ordovician continental arc on the Gondwana margin. Geol. Soc. Lond. Spec. Publ. 142, 343–367.
Pearce, J.A., Harris, N.B.W., Tindle, A.G., 1984. Trace element discrimination diagrams for the tectonic interpretation of granitic rocks. J. Pet. 25, 956–983.
Pearce, J.A., Peate, D.W., 1995. Tectonic implications of the composi tion of volcanic arc magmas. Annu. Rev. Earth Planet. Sci. 23, 251–285.
Pietranik, A., Koepke, J., 2014. Plagioclase transfer from a host granodiorite to mafic microgranular enclaves: diverse records of magma mixing. Mineral. Pet. 108, 681–694.
Poma, S., Quenardelle, S., Litvak, V., Maisonnave, E.B., Koukharsky, M., 2004. The Sierra de Macon, Plutonic expression of the Ordovician magmatic arc, Salta Province Argentina. J. South Am. Earth Sci. 16, 603–613.
Rapela, C.W., Pankhurst, R.J., Casquet, C., Baldo, E., Saavedra, J., Galindo, C., 1998. Early evolution of the proto-andean margin of south America. Geology 26, 707.
Reiners, P.W., Nelson, B.K., Ghiorso, M.S., 1995. Assimilation of felsic crust by basaltic magma: thermal limits and extents of crustal contamination of mantle-derived magmas. Geology 23, 563.
Ridolfi, F., Renzulli, A., Puerini, M., 2010. Stability and chemical equilibrium of amphibole in calc-alkaline magmas: an overview, new thermobarometric formulations and application to subduction-related volcanoes. Contrib. to Mineral. Pet 160, 45–66.
Rudnick, R.L., Fountain, D.M., 1995. Nature and Composition of the continental crust: a lower crustal perspective. Rev. Geophys. 33, 267–309.
Schmidt, M.W., 1992. Amphibole composition in tonalite as a function of pressure: an experimental calibration of the Al-in-hornblende barometer. Contrib. to Mineral. Pet 110, 304–310.
Sisson, T.W., Ratajeski, K., Hankins, W.B., Glazner, A.F., 2005. Voluminous granitic magmas from common basaltic sources. Contrib. to Mineral. Pet 148, 635–661.
Sola, A.M., 2012. Magmatismo granítico y evolución metamórfica en el ámbito de la Cordillera Oriental. Paleozoico inferior, sierra de Molinos, noroeste argentino. Ph.D. thesis. Universidad Nacional de Salta.
Sola, A.M., Becchio, R.A., Pimentel, M.M., 2013. Petrogenesis of migmatites and leucogranites from Sierra de Molinos, Salta, Northwest Argentina: a petrologic and geochemical study. Lithos 177, 470–491.
Sun, S., McDonough, W.F., 1989. Chemical and isotopic systematics of oceanic basalts: implications for mantle composition and processes. Geol. Soc. London. Spec. Publ. 42, 313–345.
Suzaño, N., Becchio, R., Nieves, A., Sola, A., Ortiz, A., 2015. Mezcla de magmas en el arco magmático Famatiniano del noroeste de Argentina: ejemplo en el complejo intrusivo Diablillos. Puna Austral. Rev. Mex. Ciencias Geol. 32, 433–454.
Vernon, R.H., 1984. Microgranitoid enclaves in granites—globules of hybrid magma quenched in a plutonic environment. Nature 309, 438–439.
Viramonte, J.M., Becchio, R.A., Viramonte, J.G., Pimentel, M.M., Martino, R.D., 2007. Ordovician igneous and metamorphic units in southeastern Puna: new U-Pb and Sm-Nd data and implications for the evolution of northwestern Argentina. J. South Am. Earth Sci. 24, 167–183.
Whitney, D.L., Evans, B.W., 2010. Abbreviations for names of rock-forming minerals. Am. Mineral. 95 (1), 185.
Wilson, M., 1989. Igneous Petrogenesis a Global Tectonic Approach, First. Ed. Springer, Netherlands, p. 466.
Zimmermann, U., 2005. Provenance studies of very low- to low-grade metasedimentary rocks of the Puncoviscana complex, northwest Argentina. Geol. Soc. Lond. Spec. Publ. 246, 381–416.
Zimmermann, U., Bahlburg, H., Mezger, K., Berndt, J., Kay, S.M., 2014. Origin and age of ultramafic rocks and gabbros in the southern Puna of Argentina: an alleged Ordovician suture revisited. Int. J. Earth Sci. 103, 1023–1036.